ATMOSPHERIC ENVIRONMENT: X 27 (2025) 100339

Contents lists available at ScienceDirect

Atmospheric Environment: X

journal homepage: www.journals.elsevier.com/atmospheric-environment-x

Comparison of modelled and experimental PM10 source contributions for mapping source-specific oxidative potential

Floris Pekel [a,*], Gaelle Uzu [b,**], Samuel Weber [b], Richard Kranenburg [a], Janot Tokaya [a], Martijn Schaap [a], Pamela Dominutti [b], Olivier Favez [c,d], Jean-Luc Jaffrezo [b], Renske Timmermans [a]

[a] TNO, Netherlands Organization for Applied Scientific Research, Department of Climate, Air and Sustainability & Department of Risk Assessment, Prevention, Innovation and Development, P.O. Box 80015, 3508 TA, Utrecht, the Netherlands
[b] Université Grenoble Alpes (UGA), CNRS, IRD, Grenoble- INP, INRAE, UMR 5001, IGE, 38402, Grenoble, France
[c] INERIS, Parc Technologique Alata, BP 2, 60550 Verneuil-en-Halatte, France
[d] Laboratoire central de surveillance de la qualité de l'air (LCSQA), 60550 Verneuil-en-Halatte, France

ARTICLE INFO

Keywords:
Particulate matter
Source attribution
Positive matrix factorization
Chemical transport model
Oxidative potential

ABSTRACT

To effectively reduce the health burden of particulate matter (PM) pollution requires indicators more directly linked to adverse health effects than total PM mass alone. Oxidative potential (OP)—the ability of PM to induce oxidative stress based on its chemical composition—is gaining recognition as a health-relevant metric. Integrating source-specific OP values from field measurements into Chemical Transport Models (CTMs) enables the mapping of source-specific OP with broad spatiotemporal coverage. A critical step is ensuring alignment between CTM-derived and observation-based source contributions.

This study evaluates and optimises the consistency between the LOTOS-EUROS CTM and Positive Matrix Factorization (PMF) source profiles, using PM10 data from 15 French sites (2013–2016). While total PM10 shows reasonable correlation with observations (r^2 = 0.35–0.66), source-specific comparisons vary across source-types and locations. Promising results are obtained for residential biomass burning (r^2 = 0.34–0.75), secondary inorganic aerosols (r^2 = 0.30–0.71), and sea salt (r^2 = 0.18–0.71), whereas road traffic shows weaker alignment (r^2 = 0.01–0.40). Using the optimized source matching, OP maps are generated over France, showing stronger contributions from anthropogenic sources to OP than to PM10 mass. The study highlights key challenges in matching CTM and PMF sources for OP modelling, due to secondary aerosol formation, source mixing within PMF profiles, and spatiotemporal representation differences.

Refining emission data, incorporating secondary organic aerosol and aging processes in CTMs, and expanding source-specific OP measurements, particularly for uncharacterized sources like agriculture are identified as essential next steps. Despite current limitations, this approach offers a promising framework for advancing health-oriented air quality management.

1. Introduction

Air pollution is one of the major environmental concerns of the 21st century due to the wide range of health impacts associated with exposure to air pollutants (Cohen et al., 2017). Exposure to outdoor air pollution is estimated to have led to 4.2 million premature deaths in 2019 worldwide (WHO, 2022). In Europe, latest estimates (EEA, 2022) indicate that at least 238.000 premature deaths in 2020 were associated with exposure to fine particulate matter (PM) concentrations above the most stringent World Health Organisation (WHO) guideline level.

Until now, air quality legislation has primarily focused on the total mass concentration of particulate matter (PM). However, PM is a complex mixture, and evidence suggests that not all PM particles pose an equal health risk with size, composition, and source playing a role (Cassee et al., 2019; Liang et al., 2022; Moreno-Ríos et al., 2022; Park et al., 2018; Valavanidis et al., 2008). To prioritise policies with the most

* Corresponding author.
** Corresponding author.
E-mail addresses: floris.pekel@tno.nl (F. Pekel), gaelle.uzu@ird.fr (G. Uzu).

https://doi.org/10.1016/j.aeaoa.2025.100339
Received 24 March 2025; Received in revised form 6 June 2025; Accepted 8 June 2025
Available online 13 June 2025

significant health impacts a shift in particulate matter (PM) regulation is needed from a mass-based to a health-relevant approach.

Whilst the exact mechanisms behind PM-induced adverse health effects have yet to be fully understood, it is generally believed that one of the toxic effects of PM is closely linked to its ability to produce reactive oxygen species (ROS) when brought into contact with human cells. Increased ROS levels lead to an imbalance between oxidant and anti-oxidant levels, triggering inflammatory responses and cellular damage which increase the risk of cardiovascular and pulmonary diseases (Crobeddu et al., 2017; Dominutti et al., 2024; Kelly and Fussell, 2015; Q. Liu et al., 2014). This ability to produce ROS is known as the oxidative potential (OP) of PM (Bates et al., 2019; Daellenbach et al., 2020; Leni et al., 2020; Uzu et al., 2011; Weichenthal et al., 2016) and has been described as a promising complementary exposure metric for health relevant PM. As recommended by the WHO, the new EU directive for the regulation of Air Quality (Directive, 2024) includes a requirement for the monitoring of OP in order to support further scientific understanding of its effect on health and the environment.

The availability of harmonized measurements of OP at a large number of locations will enable more conclusive associations between OP and health effects (Dominutti et al., 2024) and improve understanding of which particles and emitting sources are more harmful to human health. Complementing this, modelling approaches could be used to provide historical OP exposure information across wide geographic coverage, including regions without measurements, for European cohorts providing valuable data for epidemiological studies (Daellenbach et al., 2020).

In addition to improving our understanding of the health impacts of OP there is a need for source-specific OP exposure estimates to support policies aimed at protecting public health. While recent field and laboratory studies conducted in France, Spain, and Switzerland have identified residential wood burning and road traffic as major sources to OP in Western Europe (Grange et al., 2022; in 't Veld et al., 2023; Weber et al., 2021), such experimental studies are labour and resource intensive. Modelling offers a cost-effective complement, capturing key processes like transport, chemistry, and deposition to provide source-specific OP exposure maps across large regions. An additional advantage is that models also allow scenario analysis to evaluate the potential future benefits of policy measures.

To date, only a few studies have explored source-specific modelling of OP using CTMs. Bates et al. (2018) estimated OP contributions in the southeastern U.S. by linking measured OP with $PM_{2.5}$ source contributions from the CMAQ-DDM model using regression analysis, identifying biomass burning and vehicle emissions as major contributors. Daellenbach et al. (2020) combined source-specific OP values derived from field observations in Switzerland with CAMx model outputs to assess key OP sources over Europe. And recently, Vida et al. (2025) produced a first OP map for France, using an extensive dataset that overlaps with Weber et al. (2021), providing insights and challenges of determining OP exposure. These studies demonstrate the value of OP modelling by showing that key OP sources can differ from those driving PM mass concentration (Daellenbach et al., 2020; Vida et al., 2025).

In the approaches by Daellenbach et al. (2020) and Vida et al. (2025) source-specific OP maps were obtained by combining modelled PM source contributions with OP values determined in field or laboratory studies for different sources. The reliability of the results depends not only on the accuracy of the empirical source-specific OP values, but also on how well the modelled sources align with the sources for which OP values are available. Furthermore, it critically depends on the CTM's ability to accurately represent the source contributions to PM. In this study, we focus on these last two aspects - source attribution accuracy and source matching - to assess current capabilities and limitations of source-specific OP modelling. Our goal is to help define the needs for advancing OP modelling toward application in air quality management.

2. Material and methods

2.1. Experimental dataset

We have selected 13 datasets originating from the French SOURCES program (Favez et al., 2021; Weber et al., 2019, 2021). Weber et al. (2019) provides the details of the sites, the sampling periods and analytical and data processing techniques. For each station, at least one year of detailed PM chemical speciation data, mostly at a temporal frequency of every third day, was available. The station types represent urban, alpine valley, industrial, remote and traffic locations (Fig. 1). Table 1 provides the details of the sites and the sampling periods. Typically, around 160 samples were available per site for the study period 2013–2016, with a range between 38 and 240. Note that the actual number of observations used herewith refers to the paired comparison with the model results. This explains the low data use for the site of Bordeaux-Talence of about three months, while the dataset for this site covers more than one year of data (covering also 2012). A detailed set of chemical components is available for each site from off-line chemical analysis, including EC/OC (Sunset lab analyser with EUSAAR-2), Cl^-, NO_3^-, SO_4^{2-}, NH_4^+, Na^+, K^+, Mg^{2+}, and Ca^{2+}, MSA (ion chromatography), many trace elements (e.g., Al, Ca, Fe, K, As, Ba, Cd, Co, Cu, La, Mn, Mo, Ni, Pb, Rb, Sb, Sr, V, and Zn) measured by ICP-AES or ICP-MS and anhydro sugars (including levoglucosan, mannosan, arabitol, sorbitol, and mannitol) analysed using High Performance Liquid Chromatography followed by pulsed amperometric detection (HPLC-PAD).

Subsequently, Positive Matrix Factorization (PMF) was applied to derive source contributions from the PM composition dataset using the harmonized methodology and settings. The identified factors and main contributing chemicals are listed in Table 2 (Weber et al., 2019). All contributions and profile descriptions are available online at http://pmsources.u-ga.fr. Hereafter, we refer to the PMF reconstructed mass as the "observational PM data", as the difference between the actual observed PM and the PMF reconstruction is within the uncertainties of the measurement.

In further filter analyses, Weber et al. (2021) conducted measurements of OP using two complementary assays with different sensitivities regarding PM compounds (dithiothreitol, DTT, and ascorbic acid, AA). Subsequently, a weighted least squares multiple linear regression (WLS) model was used, assigning OP per μg (OP_m) to each of the sources identified with the PMF analysis. The derived OP values are included in Table 4. More details on the methodology for the OP determination and subsequent source apportionment are provided by Weber et al. (2021).

2.2. PM source apportionment using LOTOS-EUROS

In this study, we use source contributions to the PM concentrations modelled with the LOTOS-EUROS CTM and its labelling technique. LOTOS-EUROS is an open-source 3D chemistry transport model (Manders et al., 2017). It is used operationally within the Copernicus Atmospheric Modelling Service (CAMS) for the provision of air quality forecasts and PM source attribution. Primary anthropogenic PM and gaseous pollutant emissions are taken from the CAMS-REG emission inventory (Kuenen et al., 2018). Sea salt and mineral dust emissions are calculated online in the model. For inorganic aerosol chemistry, the thermodynamic equilibrium module Isorropia II (Fountoukis and Nenes, 2007) is used. The model explicitly accounts for cloud chemistry, computing sulfate formation as a function of cloud liquid water content and cloud droplet pH (Banzhaf et al., 2012). Secondary organic aerosol (SOA) is currently not modelled by default. A volatility basis set (VBS) (Donahue et al., 2006) scheme is available for LOTOS-EUROS, however, the impact of the uncertain amounts of SOA produced by the module was too small to enhance the model performance. The module is currently being revised for inclusion in newer model versions. For more details on the model and its process descriptions, we refer to Manders

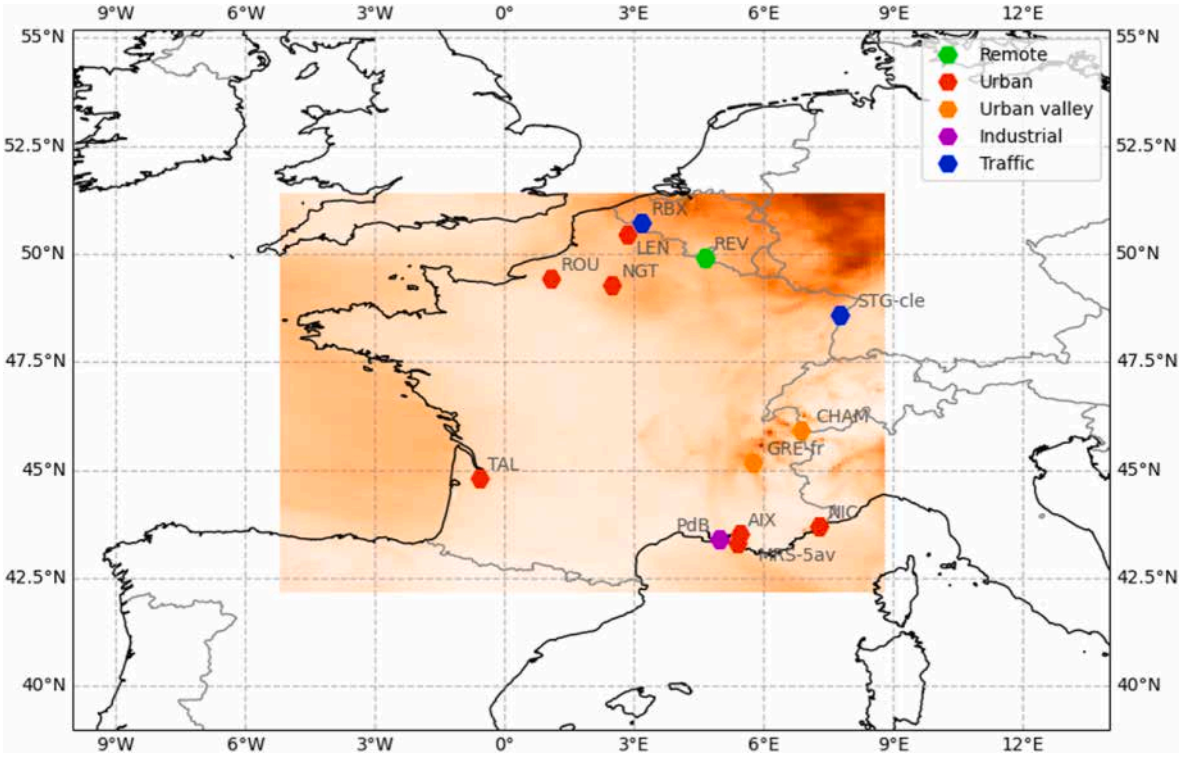

Fig. 1. Site location and France domain of LOTOS-EUROS model (background represents the mean PM10 daily concentration of the 2014-05-01, for illustration).

Table 1
Site description and sampling periods used in this study.

Name	Abbrv.	Latitude	Longitude	Altitude	Sampling period	# obs	Typology
Revin	REV	49.92	4.64	395	Jan 02, 2013 → Jun 01, 2014	168	rural
Bordeaux-Talence	TAL	44.80	−0.59	20	Jan 01, 2013 → Apr 07, 2013	38	urban background
Nice	NIC	43.70	7.29	1	Jun 04, 2014 → Jun 29, 2016	184	urban background
Marseille	MRS-5av	43.31	5.39	64	Jan 11, 2015 → Jun 27, 2016	102	urban background
Aix-en-Provence	AIX	43.53	5.44	180	Jul 18, 2013 → Jul 13, 2014	56	urban background
Nogent sur Oise	NGT	49.28	2.48	28	Jan 02, 2013 → Jun 02, 2014	155	urban background
Rouen	ROU	49.43	1.06	6	Jan 02, 2013 → Jun 01, 2014	162	urban background
Lens	LEN	50.44	2.83	47	Jan 02, 2013 → Jun 01, 2014	167	urban background
Grenoble	GRE	45.16	5.74	214	Jan 02, 2013 → Dec 29, 2014	240	urban background/alpine valley
Chamonix	CHAM	45.92	6.87	1038	Nov 02, 2013 → Oct 31, 2014	115	urban background/alpine valley
Port de Bouc	PdB	43.40	4.98	1	Jun 01, 2014 → Jun 27, 2016	185	urban background/industrial
Roubaix	RBX	50.71	3.18	10	Feb 20, 2013 → May 26, 2014	157	urban traffic
Strasbourg	STG-cle	48.57	7.75	139	Apr 02, 2013 → Apr 08, 2014	78	urban traffic

et al. (2017) and references therein.

The labelling system of LOTOS-EUROS is used to track the contribution of pre-defined source sectors or regions to the modelled particulate matter concentrations throughout a model simulation (Kranenburg et al., 2013). The labelling routine has been initially implemented for primary, inert aerosol tracers as well as chemically active tracers containing a C, N (reduced and oxidized) or S atom, as these are conserved within the chemical cycles and thus traceable. The source apportionment module for LOTOS-EUROS provides source attribution valid for current atmospheric conditions, as all chemical conversions occur under the same oxidant levels. For the semi-volatile ammonium nitrate, the source attribution is postprocessed to make sure the mass of ammonium nitrate is equally attributed to the source profile for ammonium and that of nitrate (Hendriks et al., 2013). The attribution of secondary organic aerosols is currently under development and, therefore, not included in this work. For further details and validation of this source apportionment module, we refer to (Kranenburg et al., 2013) and Timmermans et al. (2022).

The source apportionment technique in LOTOS-EUROS has been previously used to investigate the origin of particulate matter (episodes or annual averages) (Hendriks et al., 2013; Pommier et al., 2020; Pültz et al., 2023; Timmermans et al., 2017, 2022) and nitrogen dioxide (Curier et al., 2014; Schaap et al., 2013; Thürkow et al., 2023; Tokaya et al., 2024). Furthermore, it is applied in an operational setting within the CAMS policy support service (policy.atmosphere.copernicus.eu) and the TOPAS source attribution service (Topas - Air Quality Modeling).

In this study, we have applied LOTOS-EUROS version 2.2 using a nested approach. First, a European simulation was performed at ~20 × 20 km resolution using boundary conditions from the ECMWF-IFS system. A higher resolution simulation was performed over France at a resolution of ~6 × 6 km. In this way the contributions of distant sources and sources outside the European domain can be incorporated in a consistent way. Both simulations were forced using ECMWF meteorological forecast data, available on a ~9 × 9 km resolution from the operational weather forecast service. The model was applied for a 4-year period covering 2013 to 2016, using a one-month spin up period to cover the different sampling periods at the measurement stations.

Anthropogenic emissions were used from the European CAMS v4

Table 2
Identified factors and main contributing chemical species from PMF analyses performed by Weber et al. (2019).

Identified Factors	Specific Markers and Indicators	Number of sites with this factor identified
Biomass burning	Levoglucosan, Mannosan, K^+, OC, EC	13
Road traffic	EC, OC, Ba, Cr, Co, Cu, Fe, Mo, Pb, Sb, Sn, Zn	12
Nitrate rich	NO_3^-, NH_4^+	13
Sulfate rich	SO_4^{2-}, NH_4^+, Se, OC	11
Primary biogenic	Polyols	13
Marine SOA	MSA	13
Dust	Ca^{2+}, Al, Ba, Co, Cu, Fe, Mn, Pb, Sr, Ti, Zn	11
Sea-salt	Na^+, Mg^{2+}, Ca^{2+}, Cl^-	11
Aged sea-salt	Na^+, Mg^{2+}, NO_3^-, SO_4^{2-}	11
Industrial	As, Cd, Cr, Cs, Co, Ni, Pb, Rb, Se, V, Zn	3
Heavy fuel oil (HFO)	V, Ni, SO_4^{2-}, EC	5

Table 3
Labelled sources in the apportionment module of LOTOS-EUROS.

Label	Source sector	Fuel type
1	Energy	Coal
2	Energy	Biomass
3	Energy	Other fuels
4	Residential combustion	Coal
5	Residential combustion	Biomass
6	Residential combustion	Other fuels
7	Road Transport	All fuels
8	Non-road transport (incl. shipping, aviation and mobile machinery)	All fuels
9	Industry	All fuels
10	Agriculture (livestock and crop cultivation)	–
11	Other sources (oil & gas exploration and distribution, landfills and waste incineration)	All fuels
12	Natural (forest fires, sea salt, desert dust, biogenic NO)	–
13	Intercontinental/Boundary	–

emission database (Kuenen et al., 2018), with emissions detailed per fuel type for combustion sources. The inventory includes a refinement of reported residential combustion emissions following Denier Van Der Gon et al. (2015). All emissions are distributed over time using sector-specific monthly, daily and hourly time factors (Manders et al., 2017). For the residential combustion emissions, a heating degree days approach is applied (Mues et al., 2014; Simpson et al., 2012) taking into account a sliding average of the daily average temperature. When the temperatures rise above 18 °C, we assume residential combustion emissions for heating to be zero. When the sliding average temperatures drop below 18 °C the residential heating emissions will increase with decreasing temperature based on climatological temperature data. However, 20 % of all residential combustion emissions are excluded from this heating day approach, since we assume that these emissions represent non-heating emissions (e.g. cooking) and are spread evenly throughout the year. This approach was shown to be highly beneficial for solid fuel source contributions (Timmermans et al., 2022). In the source apportionment module, labels were introduced for eleven different sector-fuel combinations (see Table 3). For sectors in which several fuels are important, e.g. energy and residential, a split between the solid fuels (coal, biomass) and other fuels was made. To track all emission sources, also a label "natural" was assigned to emissions of sea salt, desert dust, forest fires from GFAS (Kaiser et al., 2012) and biogenic NO emissions. Finally, intercontinental inflow from the boundary conditions is labelled separately.

2.3. OP modelling strategy

Daellenbach et al. (2020) showed that one of the methods to achieve the modelling of oxidative potential is by assigning an intrinsic (mass normalized) OP_m to each source in a CTM model. By matching CTM source contributions to the PMF source profiles for which the OP_m values have been derived, a volume-normalized OP (OP^v) can be derived from the CTM results:

$$OP^V_{S,t} = \sum_{S,t}\left(OP_{m,S} \times C^{CTM}_{S,t}\right)$$

where OP^V (nmol min^{-1} m^{-3}) represents the OP normalized for air volume for source 'S' at time 't', OP_m (nmol min^{-1} μg^{-1}) is the intrinsic OP derived from the PMF source 'S', and C^{CTM} is the simulated mass (μg m^{-3}) of the CTM matched source 'S' at time 't'. The challenge is to properly match the CTM's sources to the PMF sources for which an OP_m has been derived.

Due to intrinsically different methodologies, the source profiles identified using PMF differ from those obtained using the CTM. The source contributions tracked in LOTOS-EUROS reflect the (grouped) source sectors provided in the input emission database (see section 2.2). Source factors identified with PMF categorize sources or species from ambient air into factors based on a large correlation in temporal behaviour. Hence, when source categories are highly correlated, they will not be separated. Moreover, PMF results often contain profiles specific for secondary PM, e.g. nitrate-rich or sulfate-rich which can encompass secondary PM from multiple sectors. The reason is that the dependencies in the chemical production cause a different temporal behaviour as compared to that of primary PM from the same sources. Based on our expertise on emission sources and an evaluation of the specific markers contained within each PMF factor we have determined which source contributions from LOTOS-EUROS would best correspond to the identified PMF profile. The resulting mapping of OP with LOTOS-EUROS based PMF profiles is provided in Table 4.

The mapping for biomass burning, road traffic and industrial may seem straightforward. However, the question rises whether the identified PMF profiles for these 3 sectors are representative of both the primary and secondary PM. The PMF factor biomass burning is largely based on the variation of levoglucosan, which is considered a robust tracer for biomass burning (Bhattarai et al., 2019). For road traffic, we considered two mapping options, considering that a significant part of the secondary nitrate from traffic could be contained in the nitrate-rich PMF profile. For the industrial factor, the chemical composition and, therewith also, the determined OP are highly variable for the three sites where the factor has been identified due to the differences in local industries. Because of the strong uncertainties associated with this PMF factor, we have excluded this source from the comparison in section 3.2.

The nitrate- and sulfate-rich profiles are identified as two stable factors by PMF that capture the majority of the secondary inorganic aerosols (SIA), without determining specific emission sources for these profiles (Weber et al., 2019). The nitrate-rich profile mainly consists of nitrate and ammonium, whereas the sulfate-rich profile is dominated by SO_4^{2-}, NH_4^+, OC and Se (Weber et al., 2019) and can cover several secondary oxidation processes (Borlaza et al., 2021). On the other hand, the labelling method assigns each secondary inorganic aerosol (NH_4NO_3 and NH_4SO_4) formed in the LOTOS-EUROS model to the originating sources of its precursors NH_3, NO_x and SO_2 (e.g. agriculture, traffic or industry in this inventory). Due to this dissimilarity, the decision was made to aggregate all mass from the nitrate-rich and sulfate-rich PMF profiles into a '*SIA-rich*' profile and match it against the total concentration of the SIA-components present in the model. For sea salt, the LOTOS-EUROS output does not distinguish between fresh and aged contributions and is therefore mapped to the total of fresh and aged sea salt PMF profile contributions. Consequently, we computed an average intrinsic OP value for the aggregated salt profiles, as well as for the

Table 4
Mapping of LOTOS-EUROS sources to PMF sources and intrinsic OP values from (Weber et al., 2021). * = 'minor' PMF profiles found at <7 stations, resulting in less power behind the OP_m. ** = the average OP_m value for the combined PMF profile for the aged and fresh sea salt profiles and the nitrate-rich and sulfate-rich profiles. Abbreviations of PM components: elemental carbon (EC), organic carbon (OC), secondary inorganic aerosols (SIA) and primary particulate matter other than EC/OC (ppm). Major components and tracers of each PMF profile are described in Table 2 and can be found in more detail in http://pmsources.u-ga.fr

PMF				LOTOS-EUROS	
Source	Specific Markers and Indicators	Intrinsic OP_m (nmol min^{-1} μg^{-1}) DTT/AA		source	PM components
Biomass burning	Levoglucosan, Mannosan, K^+, OC, EC	0.129/0.197		Energy and residential combustion, fuel type biomass	All - EC/OC/ppm/NO_3/SO_4/NH_4
Road Traffic	EC, OC, Ba, Cr, Co, Cu, Fe, Mo, Pb, Sb, Sn, Zn	0.223/0.161		Road Transport, all fuel types	Version 1 (v1) – All. Version 2 (v2): NO_3 excluded.
Industrial*	As, Cd, Cr, Cs, Co, Ni, Pb, Rb, Se, V, Zn	0.186/0. 272		Industry, all fuel types	EC/OC/ppm
Heavy fuel oil (HFO)*	V, Ni, SO_4^{2-}, EC	0.365/0.073		Non-road transport (which includes shipping)	EC/OC/ppm
Nitrate rich	NO_3^-, NH_4^+	0.044/ 0.010	0.061**/ 0.010**	All SIA species in the LOTOS-EUROS model were assigned the same OP_m	NO_3/SO_4/NH_4
Sulfate rich	SO_4^{2-}, NH_4^+, Se, OC	0.077/ 0.009			
Primary biogenic	Polyols	0.112/0.028		Not available	Not applicable
Marine SOA	MSA	0.132/−0.020		Not available	Not applicable
Dust	Ca^{2+}, Al, Ba, Co, Cu, Fe, Mn, Pb, Sr, Ti, Zn	0.121/0.037		All dust in the model	Dust
Sea salt	Na^+, Mg^{2+}, Ca^{2+}, Cl^-	0.087/ 0.062	0.062**/ 0.043**	Sea salt from natural label	Sea salt
Aged Sea Salt	Na^+, Mg^{2+}, NO_3^-, SO_4^{2-}	0.038/ 0.024			
		Assumed Intrinsic OP_m (nmol min^{-1} μg^{-1}) DTT/AA		**LOTOS EUROS source**	**PM components**
		0.129/0.197		Energy and residential combustion: non-biomass	EC/OC/ppm
		0.223/0.161		Agriculture	EC/OC/ppm
		0.129/0.197		Others (contains: Fugitives, Solvents & Waste)	EC/OC/ppm

aggregated *SIA-rich* profile (Table 4).

The issues related to this mapping will be further elaborated in our results section.

There are differences in source-specific OP_m between the two included assays (DTT and AA) due to their sensitivity to specific constituents of PM10 (Bates et al., 2019; Calas et al., 2019). In particular, the DTT test shows higher OP_m for traffic, sea salt, dust and SIA-rich sources than the AA test, while the AA test shows higher OP_m for the biomass combustion source than the DTT test. Consequently, total OP concentrations are expected to show spatial variability based on the assay used to determine the intrinsic OP of PM. This variability will be further discussed in the results.

It should be noted that for the moment, LOTOS-EUROS does not consider all the sources identified by the PMF and, vice versa, there are no intrinsic OP_m values available for the primary components of some source sectors included in the CTM. For LOTOS-EUROS these sectors are agriculture, non-biomass residential heating and energy production. As first attempt we address this issue by assigning OP_m values to the primary components – elemental carbon (EC), organic carbon (OC), and primary particulate matter (ppm) – of these CTM sources, based on the available OP_m from PMF profiles which are deemed most similar to these CTM sources (Table 4). Therefore, we applied the OP_m value from the PMF profile biomass burning to the CTM's non-biomass residential and energy combustion sector. For the SIA and dust mass fractions in these sectors, the OP_m of the SIA-rich and dust profiles are used. Finally, we assigned the OP_m of the traffic profile to the primary pollutants of the CTM's agriculture sector, since handling and transport of agricultural products also make up this source it was deemed possible that the primary pollutants (EC/OC/ppm) would largely be emitted combustion processes similar to that of road transport. But these first guess assignments of OP_m values from a different source are expected to contribute largely to the uncertainty since the sources are quite different and OP is not necessarily due to the main tracers in a source.

Conversely, a comparison between LOTOS-EUROS sources and the primary biogenic and Marine SOA PMF profiles was deemed not possible, since this LOTOS-EUROS version did not contain biogenic emissions or any SOA formation processes.

2.4. Statistical performance metrics

The LOTOS-EUROS and observational-based species concentrations and source apportionment were compared for all valid daily samples through performance indicators:

$$\text{Mean bias} = \frac{1}{N}\sum (C_{model} - C_{observation})$$

$$\text{Mean relative bias (MRB)} = \frac{1}{N}\sum \frac{C_{model} - C_{observation}}{C_{observation}}$$

$$\text{Root mean square error} = \sqrt{\frac{1}{N}\sum (C_{model} - C_{observation})^2}$$

$$\text{Temporal correlation}: r^2 = \left(\frac{\sum (C_{model} - \overline{C_{model}})(C_{observation} - \overline{C_{observation}})}{\sqrt{\sum (C_{model} - \overline{C_{model}})^2 \sum (C_{observation} - \overline{C_{observation}})^2}} \right)^2$$

For r^2, values > 0.5 are indicators of good performance, and for mean bias and RMSE, minimal values are required.

Note that for sites influenced by strong local sources, poorer model performances are expected due to representativity issues. Such sites are affected by highly variable emissions, which cannot be represented well by models with a resolution of a few kilometres. Besides increased model resolution, detailed local information on emission timing would be required. Similarly, for alpine stations (GRE and CHAM), the spatial resolution of the model and its input meteorology do not resolve specific processes (e.g. inversion layers in mountainous terrain), and are expected to lead to poorer performances. This can be seen in Fig. 3, where the performances for Chamonix, located in a narrow valley, are much lower than for Grenoble, in a more open environment.

3. Results and discussion

3.1. Comparison of concentration levels

For most stations, the modelled PM10 mass shows a good agreement with the observational data (see Fig. 2). The temporal correlation varies between 0.35 and 0.66 for the non-alpine stations. The slope of the regression (a) is systematically below 1. A lower slope value is associated with a positive value for the intercept (b), meaning that for most stations, high PM10 concentrations are underestimated while low concentrations are typically overestimated. The same behaviour is found for the majority of regression analyses for the other PM components in the model: organic carbon (OC), elemental carbon (EC), sodium (Na^+), nitrate (NO_3^-) and sulfate (SO_4^{2-}) (Fig. 3 & Table S1), indicating that the model underestimates the PM components in France and thereby the total PM10 mass. On average, a slight underestimation of observed PM10 mass is seen for all the non-alpine stations [average bias = −2,96 μg m^{-3}], except for Revin and PdB [bias = 1.02 and 0.99 μg m^{-3},

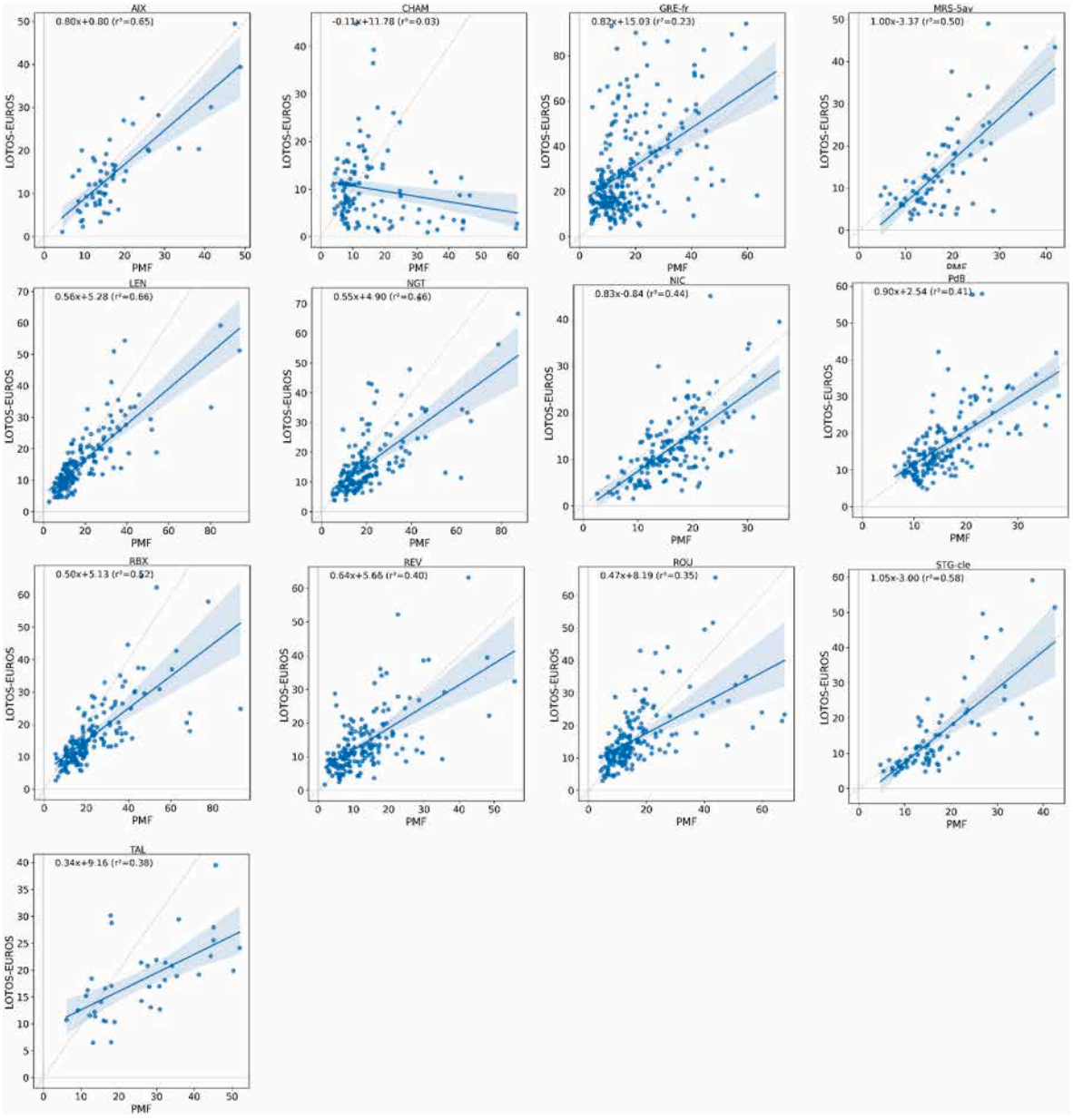

Fig. 2. a–m: Scatterplots and fits of LOTOS-EUROS PM10 versus total PM10 in PMF data for the different locations. The blue line represents the linear regression line between the LOTOS-EUROS and PMF data, while the light blue coloured areas represent the 95 % Confidence Interval surrounding this regression line.

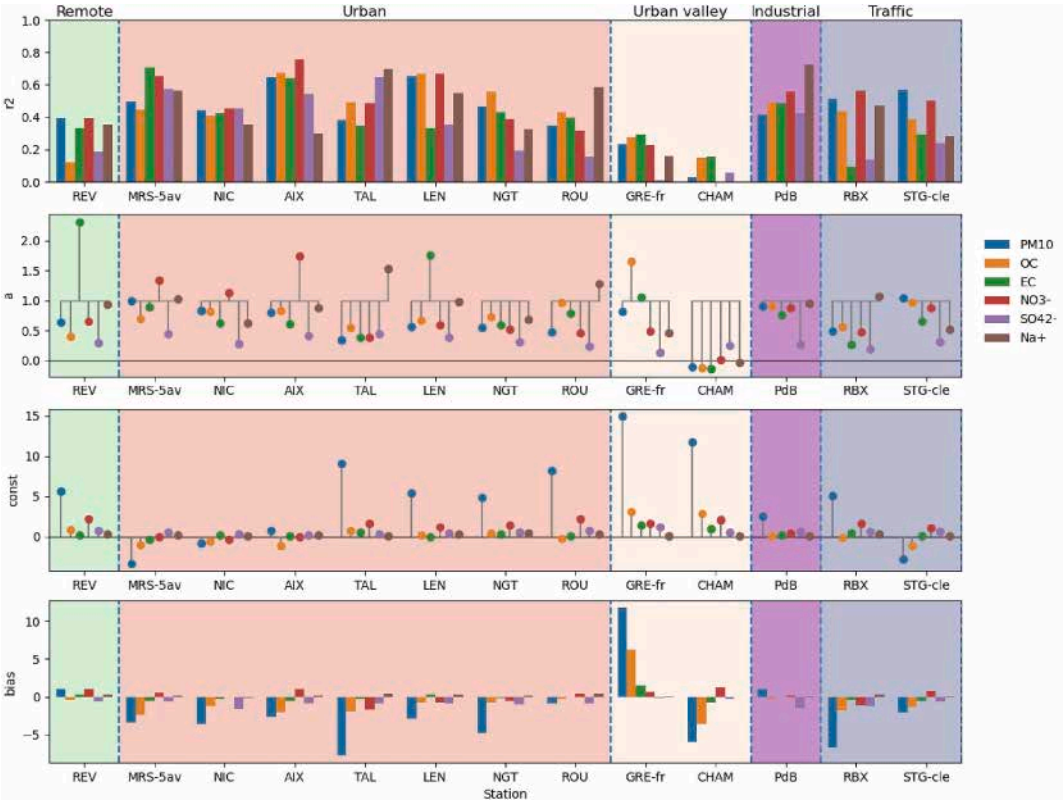

Fig. 3. Statistic of the regression of chemical species between PMF and LOTOS ($specie_{LOTOS}$ = a ×$specie_{PMF}$ + b). r^2 refers to the temporal correlation coefficient.

respectively]. The relative bias (Figure S1) ranges between −22.9 % and +28.7 %, with an average of −8 %. The PM10 mass underestimation can, to some extent, be explained by underestimations in OC, EC, and sulfate. For most of the non-alpine stations, the underestimation in OC [average bias = −1.21 μg m^{-3} or -26 %] is restricted to the summer months (not shown here), which could be due to both the formation of secondary organic aerosols and emissions of primary biogenic organic aerosols (PBOA) that are not accounted for in this LOTOS-EUROS version but do represent a large fraction of mass at this period (Bonvalot et al., 2019; Glojek et al., 2024; Golly et al., 2019; Samaké et al., 2019).

The underestimation for EC is observed for all non-alpine stations, except the two northernmost non-traffic stations (REV and LEN), which show very low observed EC concentrations (below 0.5 and 1 μg m^{-3}, respectively). LOTOS-EUROS overestimates these low EC concentrations for Lens in winter and Revin all year round (not shown here). Large underestimation and the lowest correlation are found for Roubaix, an urban traffic station [bias = −0.46 μg m^{-3}; RMB = −22 %; r^2 = 0.09], which can be expected due to representativity issues (see section 2.4). The underestimation of sulfate concentrations [average bias = −1.6 μg m^{-3}] and rather low correlation coefficient is a common feature in regional chemistry transport models (e.g. Fagerli et al., 2021; Ye et al., 2023) and is probably caused by accelerated formation of sulfate due to multiphase oxidation during severe pollution episodes (T. Liu et al., 2021; Tilgner et al., 2021; Wang et al., 2021; Ye et al., 2023) which is not yet represented in most models.

For nitrate the correlations between the modelled and observed concentrations at the non-alpine stations are moderate to good [r^2 = 0.31–0.75]. Correlation coefficients decrease with distance away from the coast. The slope is generally lower than 1 except for three stations (MRS-5av, NIC and Aix) located close to the Mediterranean coastline in the south-east of the country, which may be influenced by the formation of coarse nitrate from the heterogeneous reaction with sea salt and/or crustal dusts. Spatial heterogeneity in these comparison results may also be linked to sampling artefacts due the evaporation of ammonium nitrate at higher temperatures (Chebaicheb et al., 2024; Schaap et al., 2004).

Sodium concentrations display in general a good agreement between modelled and observed values. Correlation coefficients however decrease with distance away from the coast, probably due to uncertainties in dispersion parametrization.

The biases in the above-mentioned PM components for some stations and locations do not add up to the bias in total PM10 therefore other PM components must be missing or underestimated in the model such as the exclusion of traffic-induced resuspension of dust (and other) particles in LOTOS-EUROS, which will be elaborated upon in section 3.2.2.

3.2. *Source apportionment*

3.2.1. *Biomass burning*

The biomass burning source contributions from the PMF and the summed biomass combustion contributions from the residential and energy sectors of LOTOS-EUROS were compared. The seasonal cycles of biomass combustion, with the largest contributions during cold episodes in the winter, correspond very well, as illustrated for the station NGT in Fig. 4 (and all stations in Figure S1 in the supplementary material). This is reflected in moderate to good temporal correlation coefficients (ranging from 0.41 to 0.75), when excluding both alpine stations, Talence (which only has three months of data) and Rouen, (which misses observations during the modelled peak in winter). A clear difference at all stations is the absence of a wood combustion contribution during summer in the PMF analysis, whereas the LOTOS-EUROS model estimates some mass to the residential combustion source. Within LOTOS-EUROS, 20 % of residential combustion is estimated to be emitted by non-heating practices (e.g. cooking) and distributed evenly over the entire year (see section 2.2). From this comparison, we can conclude that either this fraction for wood combustion emissions is not attributed to the selected PMF factor or the percentage of emissions applied in

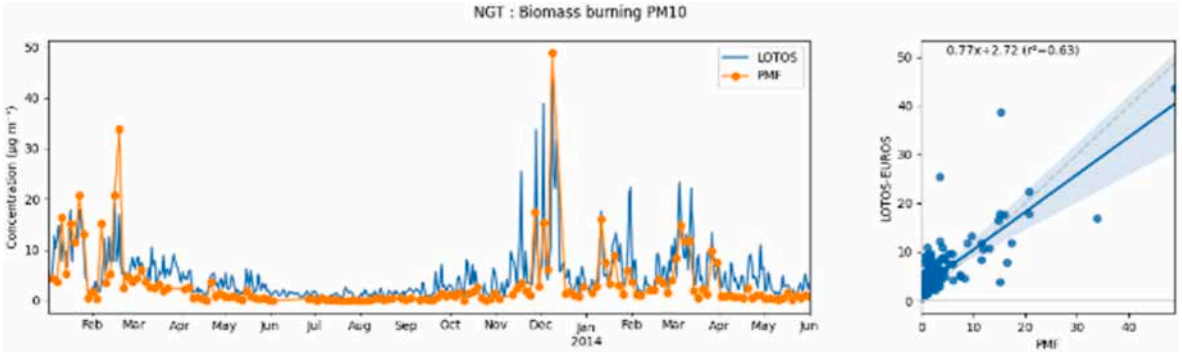

Fig. 4. Comparison of modelled biomass PM10 contribution by LOTOS-EUROS (blue) and PMF biomass combustion factor (orange) for the site of NGT. The time series and corresponding scatter plot are shown. (For interpretation of the references to colour in this figure legend, the reader is referred to the Web version of this article.)

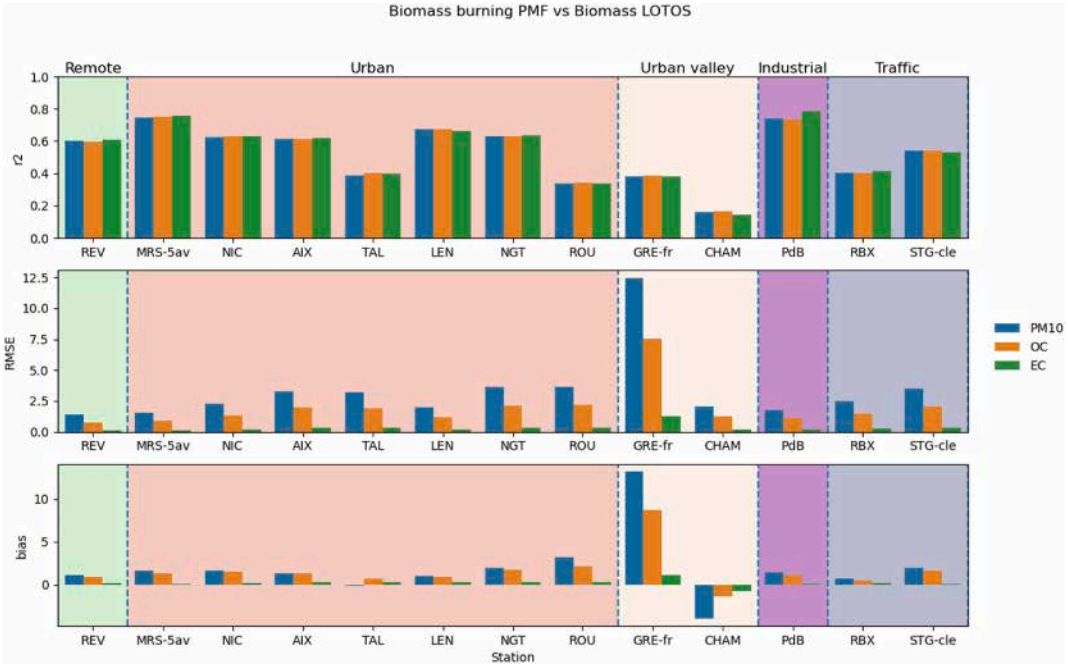

Fig. 5. Statistical comparison between the LOTOS and PMF Biomass contribution for PM10 (blue), OC (orange) and EC (green). (For interpretation of the references to colour in this figure legend, the reader is referred to the Web version of this article.)

LOTOS-EUROS for this non-heating contribution to biomass residential combustion is too large. A second possibility that partly explains the difference between LOTOS-EUROS and PMF could be the faster decay of levoglucosan at higher temperatures (in summer) (Lai et al., 2014). Since levoglucosan is used as tracer for biomass burning, this could hamper the ability of PMF to capture smaller biomass burning emissions during summer (Bhattarai et al., 2019).

The temporal correlation, bias and RMSE of this source's contribution to PM10, OC and EC are presented in Fig. 5. The absolute biomass burning contribution to PM10 apportioned by LOTOS-EUROS on average is higher than the mass contribution apportioned to this source by PMF. The same holds for the OC biomass burning contributions. The modelled "biomass" contribution is thus suspected to overestimate the contribution of this source at the national/regional scale. The positive bias is likely linked to an overestimation of the emissions. Simpson et al. (2022) developed new emission estimates (ref2v1.2) using improved estimation of fuel consumption (in particular wood) and emission factors, as well as an updated split of fuel use over different appliances and technologies. These changes lead to considerably lower wood combustion emissions for some European countries (nearly 50 % reduction for France). These ref2v1.2 emissions are now being included in updated CAMS emission inventories but were not included in this work.

Another possible reason for the bias could be that a limited part of the primary and/or secondary OC from biomass burning is distributed into other PMF factors, such as aged sea salt, PBOA, SIA-rich profiles, in the PMF analysis (see 3.2.5).

Variability in the biases across different sites may be due to uncertainties in the spatial distribution of emissions from wood burning for residential heating. These emissions are spatially attributed according to population density and the proximity of forests in the model. However, it is expected that wood heating is not widespread in the majority of buildings (except for the old buildings) in the centre of cities, but rather present in suburban housing. As a consequence, the approach followed in the model could overestimate wood burning emissions for these cities as a whole. This distribution may be improved by incorporating local information on building type and height (Manders et al., 2021). Additionally, the temporal distribution of emissions in the model does not take into account the surge in tourism during the winter period for the valley of Chamonix, which could partly explain the underestimation at this station, in combination with local temperature inversions and

Table 5
Ratio of OC/EC and OC/Levoglucosan contributions in Biomass burning and Road Traffic PMF factor. * = average and standard deviation without outliers of LEN and REV, ** = average and standard deviation are without outlier REV.

Station	Biomass burning			Road traffic	
	OC-EC ratio		OC-Levoglucosan	OC-EC ratio	
	PMF	LE	PMF	PMF	LE
AIX	7,22	6,32	5.60	1,21	0,32
CHAM	3,18	6,18	4.89	0,52	0,33
GRE-fr	3,03	6,15	4.39	1,54	0,32
LEN	60,83	6,34	6.22	3,31	0,34
MRS-5av	2,39	6,26	3.20	2,44	0,32
NGT	7,08	6,37	5.13	1,80	0,34
NIC	3,36	6,27	5.72	1,84	0,34
PdB	3,83	6,92	6.44	**NA**	0,38
RBX	9,73	6,31	7.89	0,10	0,33
REV	14,84	6,35	5.87	15,96	0,37
ROU	4,87	6,34	2.63	2,79	0,34
STG-cle	3,05	6,08	7.11	2,06	0,33
TAL	7,94	6,31	3.69	0,59	0,33
Mean	10,10 (* 5,06)	6,32	5.29	2,85 (**1,65)	0,34
Standard dev.	15,03 (*2,38)	0,19	1.52	4,24 (**1,00)	0,02

stability situations that may not be resolved by the CTM.

Interestingly, the OC-EC ratio between the PMF biomass burning factor fluctuates significantly from station to station (see Table 5), whereas this ratio is stable by parametrization for the LOTOS-EUROS source [between 6.08 and 6.92]. The EC levels for the stations LEN and REV for the biomass burning profile are substantially lower in comparison to the other stations, resulting in unexpectedly high OC-EC ratios of 14.8 and 60.83, respectively. When excluding these stations, the OC-EC ratios of the remaining stations vary between 2.39 and 9.73, which is more in line with observed biomass burning OC-EC ratios in literature (Klimont et al., 2017; Ledoux et al., 2023; Pio et al., 2011) and the values applied to the residential combustion emissions driving the LOTOS-EUROS model (Table S2). The three higher OC/EC ratio are from three sites from the north of France close to Belgium (Lens, Roubaix, Revin), the only area in France where coal burning may still have some influence on the emission. Note that the OC-EC ratios in literature are mostly for measurements directly at the emission while at the monitoring locations, the observed aged OC could be enriched by secondary formed organic matter from aging. Moreover, in Weber et al. (2019) no constraints for expected OC-EC ratios of biomass burning profiles were set in the PMF-analyses, which could help in avoiding the ratios observed here.

The OC/Levoglucosan ratios in the PMF biomass burning contributions fluctuate between 2.6 and 7.9, which is within the range of values previously reported for wood combustion measurements (Schauer et al., 2001; Schmidl et al., 2008) and the range of environmental observations (Herich et al., 2014). This variability is most probably due to uncertainties in the PMF resolving system. The range may also reflect the use of different types of wood for heating purposes, although it is expected that the woodmix seen at the sampling sites is probably not varying significantly. The inventory used in LOTOS-EUROS implicitly assumes an average mix of wood applied everywhere, a procedure that may need to be optimized depending on the availability of good proxy data for wood types.

3.2.2. Road traffic

The PMF road traffic factor was compared to the road transport contribution of LOTOS-EUROS. The statistical metrics for the comparison of this source's contribution to PM10, OC, and EC are presented in Fig. 6. Fig. 6 contains two versions of PM10: PM10 version 1 (PM10 v1) which includes all model components that are labelled within road traffic, and PM10 version 2 (PM10 v2) which excludes nitrate from the labelling. PM10 v2 has been included because, for 7 out of 12 stations, none to a very limited amount of nitrate is contributing to the PMF traffic profile (not shown); even when measured nitrate concentrations can be substantial at these stations (>10 μg m^{-3}). At these stations, the majority of the nitrate is attributed to the nitrate-rich profile. Average annual LOTOS-EUROS nitrate contributions to the traffic source range from 0.52 to 1.45 μg m^{-3}, whereas nitrate contributions in the PMF traffic profile range from 0 to 0.38 μg m^{-3}. This highlights the importance of separately evaluating the contributions of the different species per source.

Excluding nitrate from the road transport label improves the temporal correlation between the mass contributions of LOTOS-EUROS and PMF for the majority of stations. Overall, r^2 value improved by 0.08, with the stations TAL and ROU showing the largest improvements (increase r^2 by 0.24). Moreover, for all stations, the RMSE decreased from

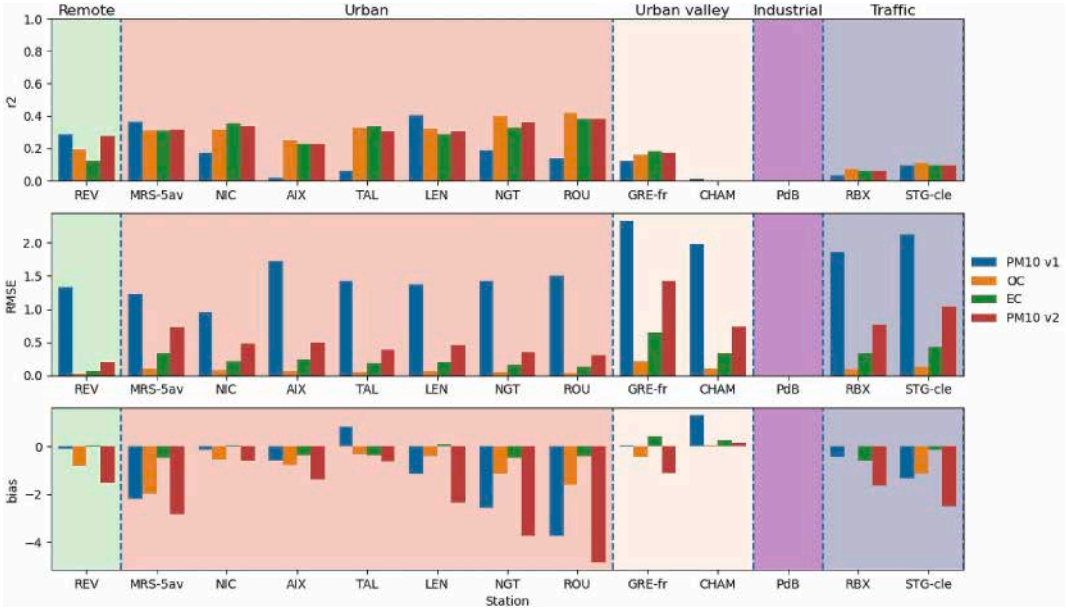

Fig. 6. Statistical comparison between the LOTOS and PMF road traffic contribution for OC, EC and the two versions of PM10.

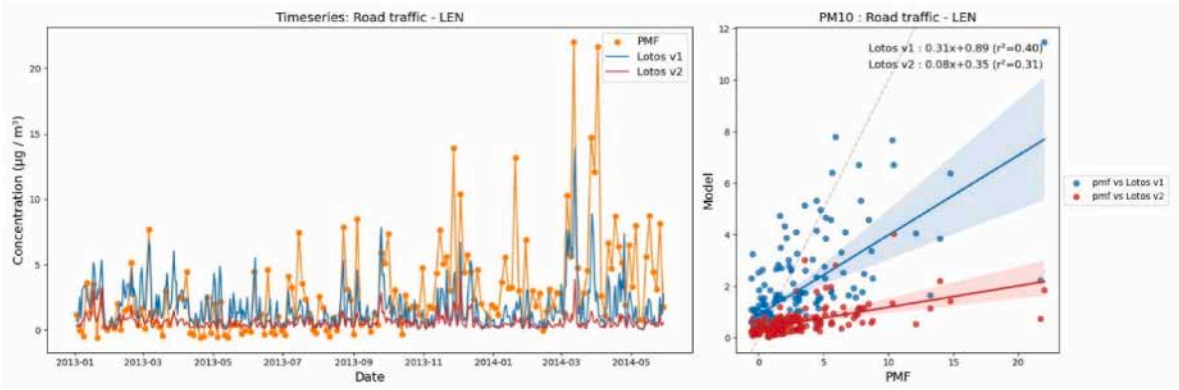

Fig. 7. Time series of PM10 contribution for the LOTOS-EUROS road traffic label version 1 (blue line), version 2 (red) and PMF road traffic factor (orange line) for the site of LEN.

version 1 (RMSE: 0.95–2.33) to the alternative version 2 (RMSE: 0.19–1.42). However, since LOTOS-EUROS version 1 already showed lower average PM10 mass contributions from road traffic than PMF, excluding nitrate further increases the negative bias (from −0.83 to −1.91 on average).

For those stations with larger nitrate contributions in the PMF road traffic profile, such as Lens, the PMF road traffic contributions show a similar peak to LOTOS-EUROS in spring (see Fig. 7 & S.2). This peak is associated with the formation of secondary ammonium nitrate from the NO_x emissions from road traffic, in combination with NH_3 emissions from the agricultural sector, which also peak in spring.

The temporal correlation between PMF and LOTOS-EUROS is low to moderate, with r^2 values below 0.4 for PM10, OC and EC. The low correlation observed at all stations indicates that modelling the highly variable traffic contributions in a time-consistent manner is challenging with either of the two approaches used here. This is consistent with a similar comparison study conducted in Germany (Timmermans et al., 2022). The fact that PM10 from road traffic can originate from either exhaust emissions, non-exhaust emissions (brake and tire wear) and the resuspension of road dust plays a role here. This is reflected in the lowest temporal PM10 correlation being observed where the PMF profiles show larger contributions from road dust (not shown here).

This LOTOS-EUROS run did not include the resuspension of traffic-related particles, which likely explains the overall underestimation compared to the PMF profile. Especially since resuspension can contribute significantly to PM10, at traffic-dominated locations. Literature findings estimate that the contribution of resuspension to PM10 concentrations ranges from 13 % (Amato et al., 2016) up to 43 % (Kupiainen et al., 2016) at road-sites in Paris and Helsinki, respectively. Estimates of resuspension contribution variy strongly per study and are highly dependent on the measurement technique, period and, site-topology (Casotti Rienda and Alves, 2021; Charron et al., 2019; Lawrence et al., 2016).

No distinction between exhaust and non-exhaust contributions is available in the PMF analysis of this study. This distinction would require the measurement of specific tracers, such as trace metals for the brake wear and crustal elements, however due to collinearity between emission sources it will remain challenging to differentiate these sources with PMF. Another factor affecting the results is the effect of temperature on the exhaust emissions. Several studies have shown (Borken-Kleefeld et al., 2018; Weilenmann et al., 2009) that exhaust emissions increase in colder temperatures. In this study, spatial-temporal profiles have been applied to the traffic emission inventories in LOTOS-EUROS based on average traffic intensity patterns, however they do not include this temperature dependence. Ongoing improvements to include (partly) temperature-dependent temporal emission profiles (Guevara et al., 2021; Mues et al., 2014) are expected to enhance the representation of modelled traffic concentrations for the newer version of the model.

The largest biases are found at NGT, MRS-5av, and ROU. The ROU station, classified as an urban background site, may not be well represented due to the model's resolution, as it shows higher PMF road traffic PM10 contributions than RBX and STG-cle, both classified as traffic stations, from which one would expect a large bias. Similarly, for NGT, the PMF captures peaks with relatively high traffic PM10 contributions, which may better reflect traffic-dominated locations. These PMF traffic contributions which are not consistent with the station typology may also reflect biases – obtained for some sites and/or factors – when using a default standardized receptor modelling approach such as in Weber et al. (2019), and not a specific tailored PMF for each site.

Overall, the difference can also partly be explained by the lower estimated OC in the modelled source in comparison to the PMF traffic profile. In the modelled source label, OC makes up on average 14 % of the PM mass (approx. 0,12 µg m^{-3}). In contrast, the PMF traffic profile consists, on average, for 30 % out of OC (approx. 0,85 µg m^{-3}). The chemical profiles of the PMF analyses present noticeable variability between sites. The OC/EC fraction in the PMF traffic varies significantly, ranging from 0.1 at ROU to nearly 16 at REV, with most values falling between 1 and 3 (see Table 5). In comparison, the OC/EC ratios of the fuel emissions used in LOTOS-EUROS varies between 1.8 for gasoline and LPG fuel types, 0.5 for diesel heavy-duty and 0.3 for light-duty vehicles (Table S3). When adjusting for daily contributions of specific fuel types to the road traffic source, LOTOS-EUROS shows a relatively stable OC/EC concentration ratio, ranging from 0.32 (AIX) to 0.38 (PdB) for the non-alpine stations. In the literature, measured OC/EC ratios at roadside locations vary between 0.3 and 1.0 (Pio et al., 2011; Amato et al., 2011; Pant et al., 2017; Jafar and Harrison, 2021). Charron et al. (2019) estimated median OC/EC emission factors (EFs) for different diesel passenger cars, ranging from 0.16 (Euro 4 Diesel) to 0.61 (Euro 4 Diesel + filter), resulting in an average traffic EF of 0.44 (SD; 0.32). Jafar and Harrison (2021) showed that OC/EC ratios increased over the years for a traffic site from 0.42 (2010–2012) to 0.70 (2015–2017), likely attributed to the improvements in vehicle filter systems. Overall, the OC/EC profiles belonging to the vehicle emissions applied in LOTOS-EUROS seem to be in accordance with OC/EC ratios in literature but more representative for older vehicles without improved filters. The traffic OC/EC ratios in the PMF data for most stations lie above the literature findings for traffic site emissions, which again may be related to the formation of secondary aerosols and aging processes that increase the organic carbon mass (Suarez-Bertoa et al., 2015). Borlaza et al. (2021) indeed state that the high OC/EC ratio (16.0) observed in the road traffic profile at REV, which is located in a dense forested area suggests a strong influence from SOA, at this location instead of primary traffic aerosols. As for the biomass burning source, the REV site is also characterised with very low contributions of EC to the traffic source, which explains the high OC/EC ratios for both these sources. Weber

et al. (2019) mention a low confidence for the PMF road traffic source at this rural site.

Finally, the difference between the PMF and LOTOS-EUROS traffic contributions may also be explained by the mixing of non-road traffic sources (e.g. shipping, aviation and mobile machinery) into the identified PMF road traffic profile because of some similarity in emitted species.

3.2.3. Non-road transport

The non-road transport label in LOTOS-EUROS corresponds to summed contributions from shipping, aviation (landing and take-off only), rail transport, and other machinery. In practice, (international) shipping is the largest contributor to this non-road transport label, especially for harbour areas. In the PMF analyses, the factor named "Heavy fuel oil" (HFO) was identified for some of the (coastal) stations based on Vanadium (V) and/or Nickel (Ni) metal concentrations. For other sites, these contributions were not differentiated from the road traffic profile, in which the V and Ni contributions ended up, which may partly explain the differences discussed in the previous section. International shipping and oil refineries are suspected to be the main contributors to HFO combustion, which, besides V and Ni, also emit large quantities of SO_2 and NO_x from which secondary inorganic aerosols are formed (Salameh et al., 2015). As the PMF analyses mostly include the secondary aerosol contributions in the sulfate- and nitrate-rich factors, we here present an indicative comparison between the primary PM (PPM) contribution in the LOTOS-EUROS non-road transport label and the concentration of vanadium in the PMF HFO factor (see Figure S4). A moderate relationship between V in the HFO factor and ppm in LOTOS-EUROS is observed for the sites of MRS-5av ($r^2 = 0.49$, see Fig. 8), NIC ($r^2 = 0.29$) and PdB ($r^2 = 0.38$), all three being located in harbour cities with intense shipping traffic or refinery activities. It has to be noted that no V was analysed at the RBX, ROU sites and additionally no Ni and V at the REV site. Moreover, no road traffic factor was identified at PdB.

3.2.4. Sea salt

The sea salt concentration in LOTOS-EUROS is estimated as 3.26 times the sodium concentration in the model. The PMF factors for sea salt are often split in two: one factor representing the fresh sea salt (with mainly Cl- and Na+) and a second one, the aged sea salt (with less-to-no Cl-, and the presence of other ions (NO_3^-, SO_4^{2-}, Mg^{2+}, K^+, Ca^{2+}) and OC in a larger amount). We compare both the total sea salt as well as the sodium contributions for this natural source. A very good fit is seen when comparing the Na^+ contributions in LOTOS-EUROS with the Na^+ contributions in the PMF aged + fresh salt factors (Fig. 9 right plot). The temporal correlation is highest for the coastal stations TAL, PdB and MRS-5av, but also for the stations ROU and LEN (Figure S5.1 & S.5.2). Contrarily, the coastal stations AIX and NIC show lower correlations in time.

This fit of LOTOS-EUROS Na^+ to the Na^+ in PMF restricted to the sea salt factors is better than with the total observed Na+ (see section 3.1). Part of the observed Na^+ ends up in the sulfate-rich factor and marine SOA factor representing respectively the formation of sodium sulfate from the heterogenous reaction of sodium with sulfate and the reaction of sodium with marine biogenic aerosols. Neither of these processes are included in LOTOS-EUROS.

For most stations, the total PM in the PMF aged and fresh sea salt factors is higher than the total LOTOS-EUROS sea salt (Fig. 9 left plot). This is related to the mixture of sea salt with ions and OC from other sources present in the aged sea salt factor. In LOTOS-EUROS aging of sea salt is included through the heterogenous reaction of sea salt with HNO_3. However, the source attribution in LOTOS-EUROS currently does not differentiate between fresh and aged sea salt preventing a matching with the separate sea salt profiles from the PMF.

The OC and other ions included in the aged sea salt factor are possibly part of some of the other labels in LOTOS-EUROS, such as shipping, thereby leading to lower contributions than calculated with PMF.

3.2.5. Mineral dust

The mineral dust contributions are compared using the PMF factor "Dust" and the total dust in the LOTOS-EUROS model. In LOTOS-EUROS mineral dust coming through the lateral boundaries of the model domain is determined, while the anthropogenic emissions from agricultural activity and road resuspension were excluded.

As illustrated by the remote station of REV, the LOTOS-EUROS model is sometimes able to accurately represent dust peaks identified in the PMF dust profile, in terms of both timing and amplitude (Fig. 10, top plot). A large dust event at the beginning of April 2014, which is also captured by the model for other locations, reflects the long-range transport of dust from the African continent. However, in some other cases, LOTOS-EUROS is showing dust peaks with moderate amplitudes, which are not visible in the PMF results (Fig. 10, bottom plot for site PdB, and Figure S6 for other stations). These discrepancies may arise because the sampling frequency of the filters used in the PMF may prevent distinguishing all local features or small events that LOTOS-EUROS, with its hourly resolution, is able to resolve. In addition, some of the spikes in the PM observations may have been intentionally excluded from the analysis, being considered as extreme events that the PMF is not able to resolve. The dust peaks present in LOTOS-EUROS for PdB are also detected for the other Mediterranean coastal stations, MRS-5av and Nice, indicating these peaks are actually due to the transport of dust from more distant sources.

3.2.6. Primary biogenic organic aerosols

The primary biogenic organic aerosol (PBOA) factor identified in the PMF shows largest contributions in summer and fall (Samaké et al., 2019; Weber et al., 2019), making up to 20 % of the total PM10 for the

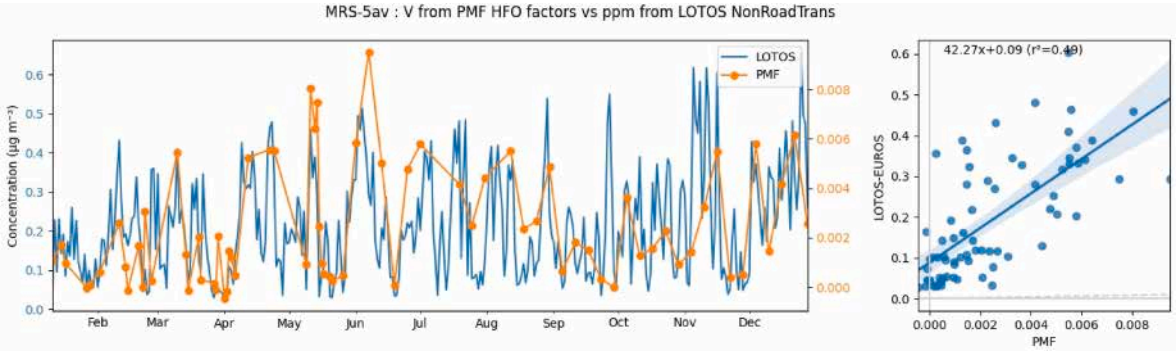

Fig. 8. Time series of the contribution of the LOTOS-EUROS non-road transport primary particulate matter (ppm) contribution against the Vanadium concentration in the PMF Heavy fuel oil factor (HFO) for the site of Marseille.

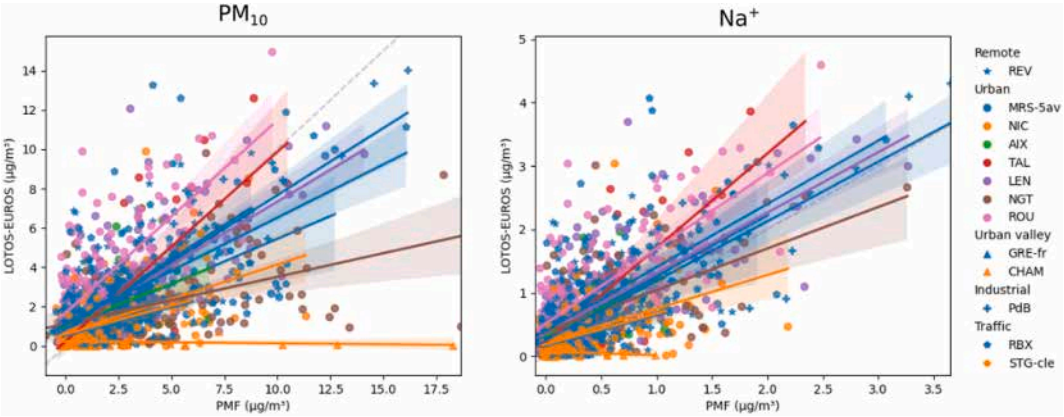

Fig. 9. LOTOS-EUROS total sea salt versus PMF aged + fresh salt contribution (left plot) and LOTOS-EUROS Na + versus Na+ in PMF aged + fresh salt contribution (right plot). Each line represents the linear regression line corresponding to comparisons at each specific station. The coloured areas around the lines represent the confident intervals.

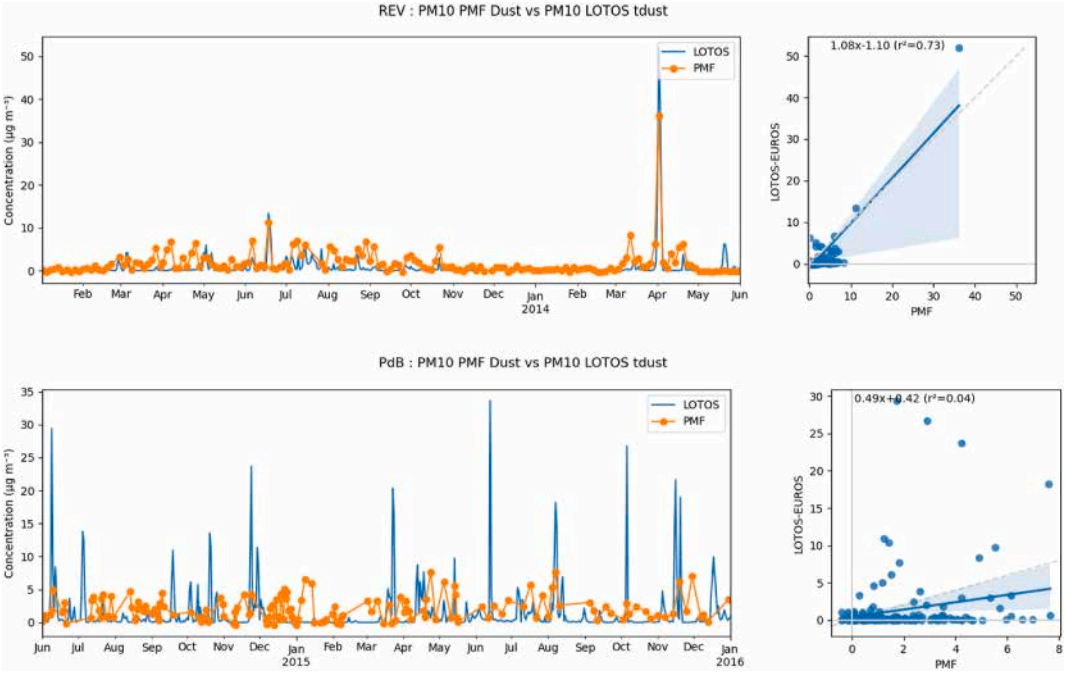

Fig. 10. Time series contribution of PM10 Dust for LOTOS-EUROS (blue line) and PMF Dust factor (orange line) for the site of Revin (top plot) and Port-de-Bouc (lower plot).

non-alpine stations, which have been linked in France to direct biological emission (Samaké et al., 2019), sometimes potentially related to agricultural activities (Golly et al., 2019; Samaké et al., 2019).

Primary biogenic emissions from land management are currently not implemented in LOTOS-EUROS and could explain part of the underestimation of PM10 by the model shown in section 3.1. Several parametrisations for emissions of fungal spores are available (Heald and Spracklen, 2009; Hoose et al., 2010; Hummel et al., 2015; Janssen et al., 2021; Sesartic and Dallafior, 2011) which have been implemented in atmospheric models (Hummel et al., 2015; Janssen et al., 2021; Vida et al., 2024). Vida et al. (2024) implemented fungal spore emissions in the CHIMERE CTM and compared modelled concentrations to the PMF PBOA data, which we have used in our study. A good performance was found over northern and eastern France, but underestimation for Mediterranean areas indicated missing sources of spores or missing factors influencing emissions. Furthermore, while monthly average results are good, differences in temporal evolution of the PBOA PMF contribution for the different sites indicate that it may be complex to incorporate primary biogenic emissions with the correct high-resolution temporal distribution.

Some sites (AIX, CHAM, MRS-5av) also show increased PBOA contributions in spring, which align with primary PM emissions from agriculture in the LOTOS-EUROS model (Figure S8). This suggests that the PMF PBOA data could potentially be used for evaluating and improving temporal distributions of agricultural activities in the model, however this pattern is not consistent between sites.

3.2.7. *Nitrate & sulfate rich*

When comparing the *SIA-rich* PM10 mass against the LOTOS-EUROS SIA concentrations, a relatively good fit for most non-Alpine stations is observed, with intermediate to good correlations for the total PM mass ($r^2_{mean} = 0.51$, range = 0.30–0.71) as well as for the individual species: nitrate ($r^2_{mean} = 0.52$, range = 0.3–0.76), ammonium ($r^2_{mean} = 0.52$, range = 0.31–0.73), and to a lesser extent sulfate ($r^2_{mean} = 0.32$, range =

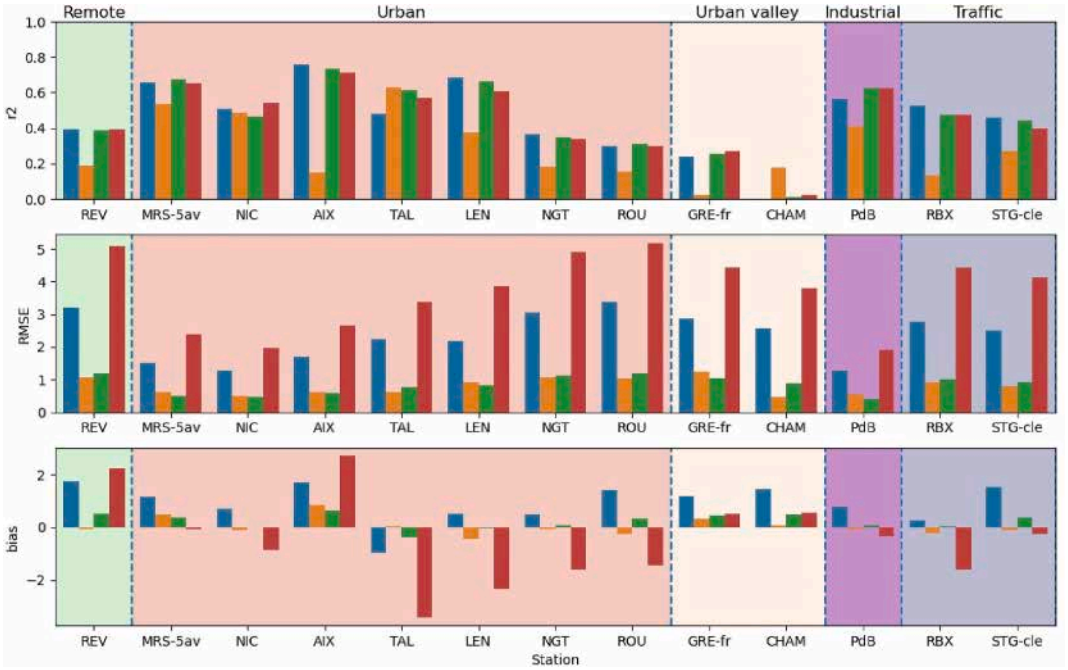

Fig. 11. Fit of SIA components in Lotos-Euros against nitrate- & sulfate-rich PMF contributions. Nitrate (Blue), sulfate (orange), ammonium (green) and the total PM10 of the nitrate- & sulfate-rich PMF profiles against the total mass of all SIA components (red) are shown.

0.13–0.63), within these source contributions (Fig. 11). The PMF profile Nitrate-rich is found for all sites, while in AIX and TAL no Sulfate-rich factor is found, resulting in relatively low sulfate concentrations in the aggregated SIA-rich profile (merely consisting out of the nitrate-rich profile for these locations). For the AIX site, the majority of the measured sulfate (approx. 58 %) was included in a local sulfate-rich/HFO profile, which likely explains the low r^2 of 0.15 for sulfate at this station.

Where LOTOS-EUROS, in general, underestimates total measured nitrate and sulfate concentrations (Section 3.1), the current comparison restricted to the SIA-rich profiles shows nitrate concentrations of a similar magnitude or a slight overestimation of the model for nitrate or sulfate (Fig. 11). This can be expected since only a percentage of the SIA is explained by the SIA-rich profiles and differs substantially between locations. On average, the SIA-rich profiles explain 81.5 %, 67.8 %, and 54,7 % of the total measured ammonium, nitrate, and sulfate concentrations, respectively. The remainder of the SIA concentrations is mostly explained by other PMF profiles; '*aged sea salt*' and '*HFO*' or the '*Marine SOA*' which has been identified for some sites (Borlaza et al., 2021; Weber et al., 2021). This may also explain the lower correlation for sulfate shown in Fig. 11.

On the other hand, the comparison also shows the effect of other species on the total mass of the PMF SIA-rich contributions. In the sulfate-rich profiles, a noticeable contribution of OC (18.4 %, SD; 7.1 %) is found (see Table S4), which can be attributed to the formation of secondary organic species (Weber et al., 2019). This could be the result of similarity in oxidation processes leading to both SOA and SIA, as suggested by the presence of some secondary biogenic species partly included in the SIA-rich profiles. Note that this is particularly the case when no specific tracers of secondary biogenic fraction are not included in the input data of the PMF (Borlaza et al., 2021).

These results underline one of the main limitations of the PMF method: its difficulty in many cases to attribute secondary species to the initial precursor source sectors, while simultaneously capturing the secondary aerosol formation in clear self-contained secondary profiles. This limitation arises from the temporal collinearity produced by the simultaneous oxidation processes of these species during aging. This can only be partially overcome with additional specific secondary tracers, as exemplified in (Glojek et al., 2024). In most cases, the secondary inorganic aerosols are captured in the nitrate- and sulfate-rich factors, but the origin of its precursors remains unclear. Depending on the site, SIA can be present in the other 'primary' or 'secondary' profiles. Conversely, other primary or secondary components are sometimes included in the SIA-rich profile, believed to be due to real mixing of species during aging, but it makes a general approach for matching with the CTM contributions complicated. Although probably too rigorous, aggregating the nitrate-rich and sulfate-rich profiles also eliminates some of the issues associated with mixed source profiles.

The comparison of the SIA time series for several sites in the North of France (e.g. LEN, NGT and RBX) shows that LOTOS-EUROS captures the increase of SIA mass observed in the spring of 2014, similar to the SIA-rich PMF profiles, but not fully capturing comparable increases in first few months of 2013 (Figure S.7). The first quarter of 2013 was characterised by low temperatures and frequent large-scale snowfalls in Northern France (Meteo-France, 2013). Cold temperatures can lead to build up of pollutants due to low vertical, and an increase in emissions (e.g. traffic (see section 3.2.2) and heating emissions). Stern et al. (2008) showed that CTMs have difficulty modelling the high concentrations for such inversion-induced winter episodes due to uncertainties for key boundary layer parameters and emissions. The temperature dependency of emissions is currently not fully represented in LOTOS-EUROS or any other CTM. However, the biomass burning contributions in LOTOS-EUROS, which do take into account the actual temperature, show increased values in the beginning of 2013.

3.3. OP modelling

Using the mapping between the PMF and LOTOS-EUROS sources (see Table 4), we are able to simulate source-specific OP from PM on a regional scale with the CTM. Fig. 12 shows the PM10 and OP maps for biomass burning, traffic, industry sources and the total (aggregated) map for France in 2014.

When moving from the PM10 mass to the OP maps, the contributions from biomass combustion (both OP_{DTT} and OP_{AA}) and traffic (OP_{DTT}) become more relevant and dominant over the source areas (road network and urban areas), which is consistent with Vida et al. (2025),

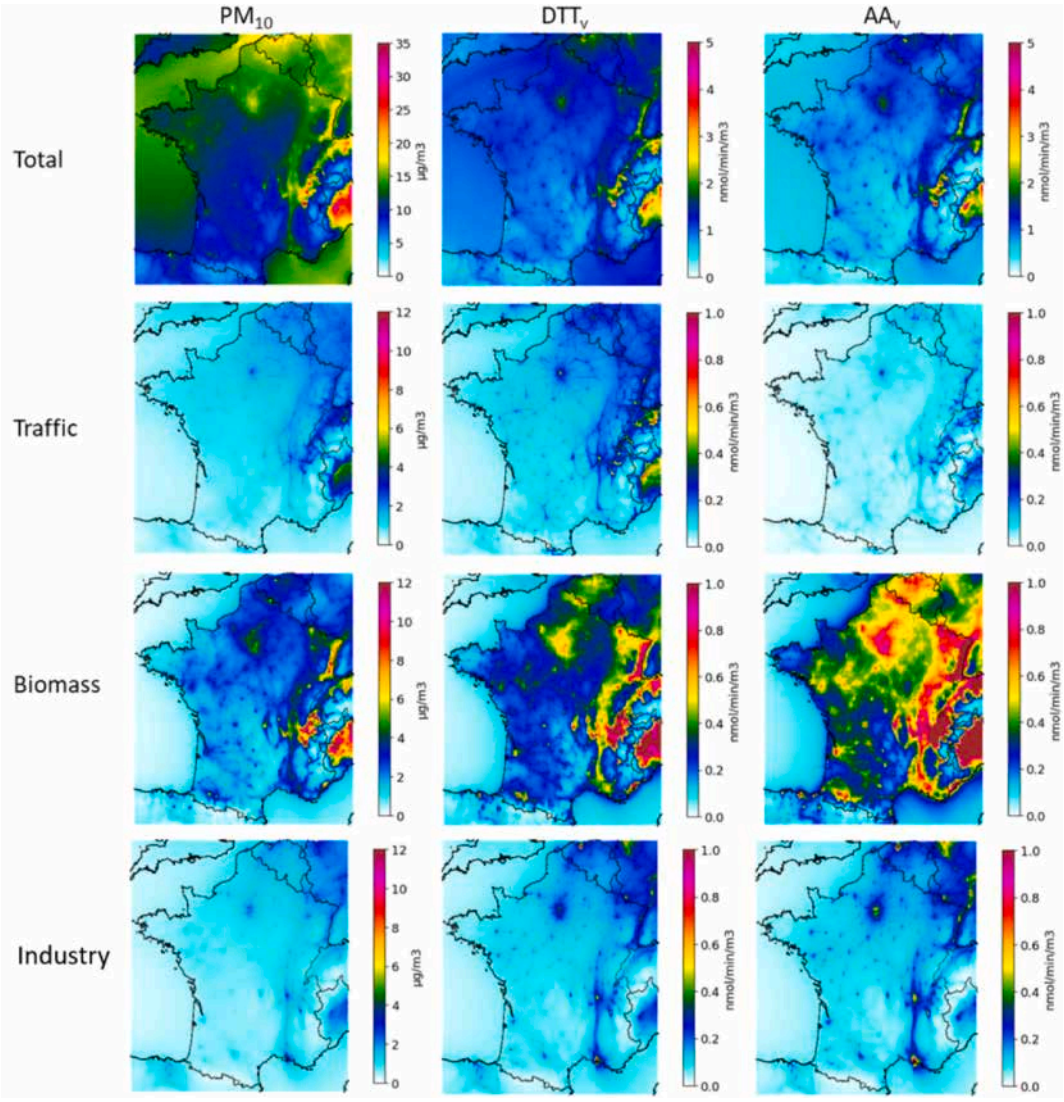

Fig. 12. a–l: PM10 concentration [µg/m^3], OP_{DTT} and OP_{AA} for the year 2014 for all aggregated PM contributions (top row; a-c) and separated into the traffic (second row; d-f), biomass combustion (third row; g-i) and industry (bottom row; j-l) contributions.

reinforcing the significance of biomass combustion and traffic sources in OP metrics. Moreover, the industrial contribution in urban areas is more highlighted in the OP maps. However, it is important to note that the industry profile is often not identified by PMF, and thus the intrinsic OP (Table 4) is based on fewer stations than the 'major' PMF sources (Weber et al., 2021).

Note also that the traffic contributions have been shown to be underestimated by the model in Section 3.2.2. While the secondary inorganic aerosols are one of the main contributors to yearly averaged PM_{10} concentrations over the country (contributes to approx. 34.3 % of PM_{10} mass), the role of SIA becomes less prominent when moving to OP (contribution of approx. 4.6 % (AA) and 22.5 % (DTT)). These results demonstrate that policy measures targeting specific sources of PM may be more efficient than those addressing total PM mass. They also underscore the necessity of incorporating health-relevant metrics, such as OP, to better represent the potential health effects of air pollution.

Several considerations should be taken into account regarding the current application of source-specific OP modelling. The average OP_m from all stations is applied to the LOTOS-EUROS source contributions, even though regional differences in OP_m for identical sources can be substantial (Daellenbach et al., 2020; Ngoc Thuy et al., 2024; Weber et al., 2021). This regional variability in OP_m may be attributed to several factors. It can be expected that chemical composition of PMF profiles differ between locations due to slight regional differences in emitting activities and meteorological conditions affecting the aging process of aerosols and thereby the OP of the PM mixture (Attah et al., 2025; Chen et al., 2020).

This also highlights that differences in the relative chemical composition between the PMF and CTM source contributions may lead to an incorrect OP value applied to the CTM source. For example, as shown in (Weber et al., 2019, 2021), the PMF nitrate- and sulfate-rich profiles also contain other species, such as a substantial OC contribution to the sulfate-profile, which likely affect the intrinsic OP assignment for these profiles. The assignment of this intrinsic OP value to the SIA contribution in the LOTOS-EUROS, which does not contain any other species, probably leads to an overestimation of the modelled SIA OP. Similar examples can be given for relative EC/OC/secondary composition differences between PMF and CTM contributions for other sources.

The variation in the source-specific OP values can also be influenced by the type of regression model. Recently, Ngoc Thuy et al. (2024) showed that the optimal regression model is dependent on the characteristics of the dataset, which can differ for each sampling location. Furthermore, source-specific OP values can be affected by interaction effects with constituents from other sources in the sample.

Laboratory-controlled studies show that synergistic or antagonistic effects between compounds can influence OP assays as well as biological interactions (Pietrogrande et al., 2022; Samake et al., 2017). However, the number of sources (i.e. independent variables) and samples per station make it difficult to include interaction effects due to the overfitting of the regression models. Note that sample handling and protocol practices are also known to influence the observed OP output (Calas et al., 2018; Dominutti et al., 2024) but are of lesser concern in this study since all samples follow a similar protocol (Weber et al., 2021).

Overall, the dynamic nature of PM composition in the atmosphere, and consequently the observed OP, brings up the challenge of assigning a single OP_m value to all CTM sources in such a way that they are representative of multiple locations and periods. A spatially and temporally dynamic OP_m estimate for emission sources and their species is important to come to a reliable ambient OP exposure that is useable in future health effect studies, although challenging to achieve. For larger-scale applications over the European domain, this requires long-term chemical speciation measurements, source attribution (e.g. through PMF) and source-specific OP analysis covering various geographical areas and site typologies.

For distinctive sources for which no intrinsic OP values are currently available, dedicated measurements and OP analyses are recommended near such sources and distant from any other major sources. For agricultural activities, some dedicated campaigns and localised measurements are ongoing to understand the variabilities of practices regarding the rural background signal (e.g. culture, livestock, agroforestry) in the Netherlands (unpublished data).

Moreover, CTM models used for OP modelling should be extended with sources and species which have been shown to have high intrinsic OP associated to them. This includes metals from non-exhaust transport emissions (Bates et al., 2019; Daellenbach et al., 2020) and (primary) biogenic organic aerosols (Samake et al., 2017; Weber et al., 2019). Although modelling studies for these PM components are being performed (Daellenbach et al., 2020; Janssen et al., 2021; Vida et al., 2024) they do not (yet) cover the whole range of relevant sources and are not as common as for other (regulated) air pollutants. Further development of accurate emission inventories or parametrisations are required to make further progress.

4. Conclusion

This study demonstrates the potential of source-specific OP modelling using CTMs at the regional scale. By focussing on a critical step in OP modelling – the accuracy of matching PM source contributions from CTM and PMF – we not only validate key aspects of the approach but also identify specific improvements required to enhance its reliability.

The generated OP maps illustrate that populations in close proximity to anthropogenic sources (particularly urban areas) are more likely to be exposed to PM mixtures with higher oxidative (re)activity. A key requirement for reliable OP modelling is the consistency between PM source contributions modelled by CTMs and those derived from observational data, both in terms of magnitude and source profile characteristics. Evaluation and optimisation of this alignment proved to be challenging due to the fundamentally different paradigms of CTMs (mechanistic, process-based) and PMF (empirical, data driven).

Our results reveal promising agreement for several sources, such as biomass burning emissions, sea salt and secondary inorganic aerosols components, validating the potential of the OP modelling approach. At the same time, the study highlights limitations and areas for further improvement in both modelling frameworks. Recommended enhancements to CTMs like LOTOS-EUROS include refinement of emissions and OC/EC emission ratios to reflect fuel shifts and technological developments, improved spatiotemporal emission distributions accounting for temperature and local practices, and incorporation of SOA production, aging of aerosols and emissions of PBOA and metal components.

A key limitation of PMF is its reduced ability to assign secondary aerosols to distinct primary sectors and to resolve minor source contributions in separate profiles, due to mixing in the atmosphere, producing co-linearity in the evolution of concentrations. The integration of CTM and PMF results facilitates the identification of primary sources (e.g. linking the PMF HFO factor to the shipping sector) and helps clarify previously unresolved sources in PMF. An important improvement would be to conduct targeted observations and PMF studies to derive source-specific OP values for currently uncharacterized sources such as agriculture.

In conclusion, despite the methodological complexity, source-specific OP modelling with CTMs shows strong potential as a tool for advancing air quality management. Future work should focus on refining both CTM and PMF, alongside extending and harmonising source-specific OP measurements across multiple locations. While further epidemiological research is needed to confirm the health relevance of these findings, this modelling framework and these developments will support more targeted and effective policies, ultimately contributing to improved air quality and public health outcomes.

CRediT authorship contribution statement

Floris Pekel: Writing – review & editing, Writing – original draft, Visualization, Methodology, Formal analysis. **Gaelle Uzu:** Writing – review & editing, Supervision, Data curation, Conceptualization. **Samuel Weber:** Software, Methodology. **Richard Kranenburg:** Software, Formal analysis. **Janot Tokaya:** Writing – review & editing, Formal analysis. **Martijn Schaap:** Writing – review & editing. **Pamela Dominutti:** Writing – review & editing. **Olivier Favez:** Writing – review & editing. **Jean-Luc Jaffrezo:** Writing – review & editing, Conceptualization. **Renske Timmermans:** Writing – review & editing, Supervision, Methodology, Conceptualization.

Funding

This work has been partly funded by the RI-urbans project which has received funding from the European Union's Horizon 2020 research and innovation program under grant agreement No 101036245. The sampling and chemical analyses performed at the REV, LEN, ROU, NGT, RBX, STG, TAL, GRE, MRS-5av, PdB, and NIC sites have been mainly funded by the French Ministry of Environment in the frame of the CARA program. Sampling at other sites, as well as analytical work on OP at AirOSol facility was notably funded through ACME IDEX projects at University Grenoble Alpes (grant no. ANR-15-IDEX-02) and PR-PRE-2021, UGA-UGA 2022-16 FUGA.

Declaration of competing interest

The authors declare that they have no known competing financial interests or personal relationships that could have appeared to influence the work reported in this paper.

Acknowledgements

The authors would like to express their sincere gratitude to many people of the Air-O-Sol analytical platform at IGE (including Sophie Darfeuil, Rhabira Elazzouzi, and Takoua Madhbi) and to all the personnel in the AASQA in charge of the sites for their contribution in conducting the dedicated sample collection.

Numerous people from French regional air quality monitoring networks (Atmo Haut-de-France, Atmo Grand-Est, Atmo Nouvelle-Aquitaine, Atmo Auvergne Rhône-Alpes and Atmo Sud) are warmly acknowledged for filter and data collection. Authors are also very thankful to Laurent Alleman and co-workers at IMT NE (Douai, France) for chemical analyses of a fraction of these filter samples.

Appendix A. Supplementary data

Supplementary data to this article can be found online at https://doi.org/10.1016/j.aeaoa.2025.100339.

Data availability

Data will be made available on request.

References

Amato, F., Favez, O., Pandolfi, M., Alastuey, A., Querol, X., Moukhtar, S., Bruge, B., Verlhac, S., Orza, J.A.G., Bonnaire, N., Le Priol, T., Petit, J.F., Sciare, J., 2016. Traffic induced particle resuspension in Paris: Emission factors and source contributions. Atmos. Environ. 129, 114–124. https://doi.org/10.1016/j.atmosenv.2016.01.022.

Amato, F., Viana, M., Richard, A., Furger, M., Prévôt, A.S.H., Nava, S., Lucarelli, F., Bukowiecki, N., Alastuey, A., Reche, C., Moreno, T., Pandolfi, M., Pey, J., Querol, X., 2011. Size and time-resolved roadside enrichment of atmospheric particulate pollutants. Atmos. Chem. Phys. 11, 2917–2931. https://doi.org/10.5194/acp-11-2917-2011.

Attah, R., Kaur, K., Reilly, C.A., Deering-Rice, C.E., Kelly, K.E., 2025. The effects of photochemical aging and interactions with secondary organic aerosols on cellular toxicity of combustion particles. J. Aerosol Sci. 183. https://doi.org/10.1016/j.jaerosci.2024.106473. June 2024.

Banzhaf, S., Schaap, M., Kerschbaumer, A., Reimer, E., Stern, R., van der Swaluw, E., Builtjes, P., 2012. Implementation and evaluation of pH-dependent cloud chemistry and wet deposition in the chemical transport model REM-Calgrid. Atmos. Environ. 49, 378–390. https://doi.org/10.1016/j.atmosenv.2011.10.069.

Bates, J.T., Fang, T., Verma, V., Zeng, L., Weber, R.J., Tolbert, P.E., Abrams, J.Y., Sarnat, S.E., Klein, M., Mulholland, J.A., Russell, A.G., 2019. Review of acellular assays of ambient particulate matter oxidative potential: methods and relationships with composition, sources, and health effects [Review-article]. Environ. Sci. Technol. 53 (8), 4003–4019. https://doi.org/10.1021/acs.est.8b03430.

Bates, J.T., Weber, R.J., Verma, V., Fang, T., Ivey, C., Liu, C., Sarnat, S.E., Chang, H.H., Mulholland, J.A., Russell, A., 2018. Source impact modeling of spatiotemporal trends in PM2.5 oxidative potential across the eastern United States. Atmos. Environ. 193, 158–167. https://doi.org/10.1016/J.ATMOSENV.2018.08.055.

Bhattarai, H., Saikawa, E., Wan, X., Zhu, H., Ram, K., Gao, S., Kang, S., Zhang, Q., Zhang, Y., Wu, G., Wang, X., Kawamura, K., Fu, P., Cong, Z., 2019. Levoglucosan as a tracer of biomass burning: recent progress and perspectives. Atmos. Res. 220, 20–33. https://doi.org/10.1016/J.ATMOSRES.2019.01.004.

Bonvalot, L., Tuna, T., Fagault, Y., Sylvestre, A., Mesbah, B.A., Wortham, H., Jaffrezo, J. L., Marchand, N., Bard, E., 2019. Source apportionment of carbonaceous aerosols in the vicinity of a Mediterranean industrial harbor: a coupled approach based on radiocarbon and molecular tracers. Atmos. Environ. 212 (March), 250–261. https://doi.org/10.1016/j.atmosenv.2019.04.008.

Borken-Kleefeld, J., Dallmann, T., Berlin, B.|, Brussels, San, Washington, F., 2018. White paper: REMOTE SENSING OF MOTOR VEHICLE EXHAUST EMISSIONS, accessible through. https://theicct.org/publication/remote-sensing-of-motor-vehicle-exhaust-emissions/.

Borlaza, L.J.S., Weber, S., Uzu, G., Jacob, V., Cañete, T., Micallef, S., Trébuchon, C., Slama, R., Favez, O., Jaffrezo, J.L., 2021. Disparities in particulate matter (PM10) origins and oxidative potential at a city scale (Grenoble, France) - Part 1: source apportionment at three neighbouring sites. Atmos. Chem. Phys. 21 (7), 5415–5437. https://doi.org/10.5194/ACP-21-5415-2021.

Calas, A., Uzu, G., Besombes, J.L., Martins, J.M.F., Redaelli, M., Weber, S., Charron, A., Albinet, A., Chevrier, F., Brulfert, G., Mesbah, B., Favez, O., Jaffrezo, J.L., 2019. Seasonal variations and chemical predictors of oxidative potential (OP) of particulate matter (PM), for seven urban French sites. Atmosphere 10 (11), 1–20. https://doi.org/10.3390/atmos10110698.

Calas, A., Uzu, G., Kelly, F.J., Houdier, S., Martins, J.M.F., Thomas, F., Molton, F., Charron, A., Dunster, C., Oliete, A., Jacob, V., Besombes, J.L., Chevrier, F., Jaffrezo, J.L., 2018. Comparison between five acellular oxidative potential measurement assays performed with detailed chemistry on PM10 samples from the city of Chamonix (France). Atmos. Chem. Phys. 18 (11), 7863–7875. https://doi.org/10.5194/ACP-18-7863-2018.

Casotti Rienda, I., Alves, C.A., 2021. Road dust resuspension: a review. Atmos. Res. 261 (March). https://doi.org/10.1016/j.atmosres.2021.105740.

Cassee, F., Morawska, L., Peters, A., Wierzbicka, A., Buonanno, G., Cyrys, J., SchnelleKreis, J., Kowalski, M., Riediker, M., Birmili, W., Querol, X., Yildirim, A.Ö., Elder, A., Yu, I.J., Øvrevik, J., Hougaard, K.S., Loft, S., Schmid, O., Schwarze, P.E., et al., 2019. White Paper: ambient ultrafine particles: evidence for policy makers. https://efca.net/files/WHITE%20PAPER-UFP%20evidence%20for%20policy%20makers%20(25%20OCT).pdf.

Charron, A., Polo-Rehn, L., Besombes, J.L., Golly, B., Buisson, C., Chanut, H., Marchand, N., Guillaud, G., Jaffrezo, J.L., 2019. Identification and quantification of particulate tracers of exhaust and non-exhaust vehicle emissions. Atmos. Chem. Phys. 19 (7), 5187–5207. https://doi.org/10.5194/acp-19-5187-2019.

Chebaicheb, H., De Brito, J.F., Amodeo, T., Couvidat, F., Petit, J.E., Tison, E., Abbou, G., Baudic, A., Chatain, M., Chazeau, B., Marchand, N., Falhun, R., Francony, F., Ratier, C., Grenier, D., Vidaud, R., Zhang, S., Gille, G., Meunier, L., et al., 2024. Multiyear high-temporal-resolution measurements of submicron aerosols at 13 French urban sites: data processing and chemical composition. Earth Syst. Sci. Data 16 (11), 5089–5109. https://doi.org/10.5194/essd-16-5089-2024.

Chen, Z., Chen, D., Zhao, C., Kwan, M. po, Cai, J., Zhuang, Y., Zhao, B., Wang, X., Chen, B., Yang, J., Li, R., He, B., Gao, B., Wang, K., Xu, B., 2020. Influence of meteorological conditions on PM2.5 concentrations across China: a review of methodology and mechanism. Environ. Int. 139 (February). https://doi.org/10.1016/j.envint.2020.105558.

Cohen, A.J., Brauer, M., Burnett, R., Anderson, H.R., Frostad, J., Estep, K., Balakrishnan, K., Brunekreef, B., Dandona, L., Dandona, R., Feigin, V., Freedman, G., Hubbell, B., Jobling, A., Kan, H., Knibbs, L., Liu, Y., Martin, R., Morawska, L., et al., 2017. Estimates and 25-year trends of the global burden of disease attributable to ambient air pollution: an analysis of data from the Global Burden of Diseases Study 2015. Lancet 389 (10082), 1907–1918. https://doi.org/10.1016/S0140-6736(17)30505-6.

Crobeddu, B., Aragao-Santiago, L., Bui, L.C., Boland, S., Baeza Squiban, A., 2017. Oxidative potential of particulate matter 2.5 as predictive indicator of cellular stress. Environ. Pollut. 230, 125–133. https://doi.org/10.1016/J.ENVPOL.2017.06.051.

Curier, R.L., Kranenburg, R., Segers, A.J.S., Timmermans, R.M.A., Schaap, M., 2014. Synergistic use of OMI NO2 tropospheric columns and LOTOS-EUROS to evaluate the NOx emission trends across Europe. Rem. Sens. Environ. 149 (2), 58–69. https://doi.org/10.1016/j.rse.2014.03.032.

Daellenbach, K.R., Uzu, G., Jiang, J., Cassagnes, L.E., Leni, Z., Vlachou, A., Stefenelli, G., Canonaco, F., Weber, S., Segers, A., Kuenen, J.J.P., Schaap, M., Favez, O., Albinet, A., Aksoyoglu, S., Dommen, J., Baltensperger, U., Geiser, M., El Haddad, I., et al., 2020. Sources of particulate-matter air pollution and its oxidative potential in Europe. Nature 587 (7834), 414–419. https://doi.org/10.1038/S41586-020-2902-8.

Denier Van Der Gon, H.A.C., Bergström, R., Fountoukis, C., Johansson, C., Pandis, S.N., Simpson, D., Visschedijk, A.J.H., 2015. Particulate emissions from residential wood combustion in Europe - revised estimates and an evaluation. Atmos. Chem. Phys. https://doi.org/10.5194/acp-15-6503-2015.

Directive (EU) 2024/2881 of the European Parliament and of the Council of 23 October 2024 on Ambient Air Quality and Cleaner Air for Europe (Recast), 2024, p. 2881. https://eur-lex.europa.eu/eli/dir/2024/2881/oj/eng.

Dominutti, P.A., Jaffrezo, J., Marsal, A., Mhadhbi, T., Elazzouzi, R., 2024. An interlaboratory comparison to quantify oxidative potential measurement in aerosol particles : challenges and recommendations for harmonisation. Atmospheric Measurement Techniques Discussions 1–32. July. https://amt.copernicus.org/preprints/amt-2024-107/.

Donahue, N.M., Robinson, A.L., Stanier, C.O., Pandis, S.N., 2006. Coupled partitioning, dilution, and chemical aging of semivolatile organics. Environ. Sci. Technol. 40 (8), 2635–2643. https://doi.org/10.1021/ES052297C/SUPPL_FILE/ES052297CSI20060116_103641.PDF.

EEA, 2022. Air quality in europe 2022. https://www.eea.europa.eu/publications/air-quality-in-europe-2022.

Fagerli, H., Basart, S., CAMS 61 team, 2021. Evaluation of PM and its Chemical Components Modelled by Regional Models in CAMS.

Favez, O., Weber, S., Petit, J.E., Alleman, L.Y., Albinet, A., Riffault, V., Chazeau, B., Amodeo, T., Salameh, D., Zhang, Y., Srivastava, D., Samaké, A., Aujay-Plouzeau, R., Papin, A., Bonnaire, N., Boullanger, C., Chatain, M., Chevrier, F., Detournay, A., et al., 2021. Overview of the French operational network for in situ observation of PM chemical composition and sources in urban environments (CARA program). Atmosphere 12 (2). https://doi.org/10.3390/atmos12020207.

Fountoukis, C., Nenes, A., 2007. ISORROPIAII: a computationally efficient thermodynamic equilibrium model for K+-Ca2+-Mg2+-NH4 +-Na+-SO42–NO3 –Cl–H2O aerosols. Atmos. Chem. Phys. 7 (17), 4639–4659.

Glojek, K., Dinh Ngoc Thuy, V., Weber, S., Uzu, G., Manousakas, M., Elazzouzi, R., Džepina, K., Darfeuil, S., Ginot, P., Jaffrezo, J.L., Žabkar, R., Turšič, J., Podkoritnik, A., Močnik, G., 2024. Annual variation of source contributions to PM10 and oxidative potential in a mountainous area with traffic, biomass burning, cement-plant and biogenic influences. Environ. Int. 189 (March). https://doi.org/10.1016/j.envint.2024.108787.

Golly, B., Waked, A., Weber, S., Samake, A., Jacob, V., Conil, S., Rangognio, J., Chrétien, E., Vagnot, M.P., Robic, P.Y., Besombes, J.L., Jaffrezo, J.L., 2019. Organic markers and OC source apportionment for seasonal variations of PM2.5 at 5 rural sites in France. Atmos. Environ. 198 (September 2018), 142–157. https://doi.org/10.1016/j.atmosenv.2018.10.027.

Grange, S.K., Uzu, G., Weber, S., Jaffrezo, J.L., Hueglin, C., 2022. Linking Switzerland's PM10 and PM2.5 oxidative potential (OP) with emission sources. Atmos. Chem. Phys. 22 (10), 7029–7050. https://doi.org/10.5194/ACP-22-7029-2022.

Guevara, M., Jorba, O., Tena, C., Denier Van Der Gon, H., Kuenen, J., Elguindi, N., Darras, S., Granier, C., Pérez García-Pando, C., 2021. Copernicus Atmosphere Monitoring Service TEMPOral profiles (CAMS-TEMPO): global and European emission temporal profile maps for atmospheric chemistry modelling. Earth Syst. Sci. Data 13 (2), 367–404. https://doi.org/10.5194/ESSD-13-367-2021.

Heald, C.L., Spracklen, D.V., 2009. Atmospheric budget of primary biological aerosol particles from fungal spores. Geophys. Res. Lett. 36 (9). https://doi.org/10.1029/2009GL037493.

Hendriks, C., Kranenburg, R., Kuenen, J., van Gijlswijk, R., Wichink Kruit, R., Segers, A., Denier van der Gon, H., Schaap, M., 2013. The origin of ambient particulate matter concentrations in The Netherlands. Atmos. Environ. 69, 289–303. https://doi.org/10.1016/j.atmosenv.2012.12.017.

Herich, H., Gianini, M.F.D., Piot, C., Močnik, G., Jaffrezo, J.L., Besombes, J.L., PrévÔt, A. S.H., Hueglin, C., 2014. Overview of the impact of wood burning emissions on carbonaceous aerosols and PM in large parts of the alpine region. Atmos. Environ. 89, 64–75. https://doi.org/10.1016/j.atmosenv.2014.02.008.

Hoose, C., Kristjánsson, J.E., Burrows, S.M., 2010. How important is biological ice nucleation in clouds on a global scale? Environ. Res. Lett. 5 (2). https://doi.org/10.1088/1748-9326/5/2/024009.

Hummel, M., Hoose, C., Gallagher, M., Healy, D.A., Huffman, J.A., O'Connor, D., Pöschl, U., Pöhlker, C., Robinson, N.H., Schnaiter, M., Sodeau, J.R., Stengel, M., Toprak, E., Vogel, H., 2015. Regional-scale simulations of fungal spore aerosols using an emission parameterization adapted to local measurements of fluorescent biological aerosol particles. Atmos. Chem. Phys. 15 (11), 6127–6146. https://doi.org/10.5194/ACP-15-6127-2015.

in 't Veld, M., Pandolfi, M., Amato, F., Pérez, N., Reche, C., Dominutti, P., Jaffrezo, J., Alastuey, A., Querol, X., Uzu, G., 2023. Discovering oxidative potential (OP) drivers of atmospheric PM10, PM2.5, and PM1 simultaneously in North-Eastern Spain. Sci. Total Environ. 857. https://doi.org/10.1016/J.SCITOTENV.2022.159386.

Jafar, H.A., Harrison, R.M., 2021. Spatial and temporal trends in carbonaceous aerosols in the United Kingdom. Atmos. Pollut. Res. 12 (1), 295–305. https://doi.org/10.1016/j.apr.2020.09.009.

Janssen, R., Heald, C.L., Steiner, A.L., Perring, A.E., Alex Huffman, J., Robinson, E.S., Twohy, C.H., Ziemba, L.D., 2021. Drivers of the fungal spore bioaerosol budget: observational analysis and global modeling. Atmos. Chem. Phys. 21 (6), 4381–4401. https://doi.org/10.5194/ACP-21-4381-2021.

Kaiser, J.W., Heil, A., Andreae, M.O., Benedetti, A., Chubarova, N., Jones, L., Morcrette, J.-J., Razinger, M., Schultz, M.G., Suttie, M., van der Werf, G.R., 2012. Biomass burning emissions estimated with a global fire assimilation system based on observed fire radiative power. Biogeosciences 9 (1), 527–554. https://doi.org/10.5194/bg-9-527-2012.

Kelly, F.J., Fussell, J.C., 2015. Linking ambient particulate matter pollution effects with oxidative biology and immune responses. Ann. N. Y. Acad. Sci. 1340 (1), 84–94. https://doi.org/10.1111/nyas.12720.

Klimont, Z., Kupiainen, K., Heyes, C., Purohit, P., Cofala, J., Rafaj, P., Borken-Kleefeld, J., Schöpp, W., 2017. Global anthropogenic emissions of particulate matter including black carbon. Atmos. Chem. Phys. 17 (14), 8681–8723. https://doi.org/10.5194/acp-17-8681-2017.

Kranenburg, R., Segers, A.J.J., Hendriks, C., Schaap, M., 2013. Source apportionment using LOTOS-EUROS: module description and evaluation. Geosci. Model Dev. (GMD) 6 (3), 721–733. https://doi.org/10.5194/gmd-6-721-2013.

Kuenen, J., Dellaert, S., Visschedijk, A., Jonkers, S., Jalkanen, J., Denier van der Gon, H., 2018. Copernicus atmosphere monitoring service CAMS_81-Global and regional emissions D81.1.1.2-M12: European emissions time series (2000-2015). https://atmosphere.copernicus.eu/sites/default/files/2019-11/02_CAMS81_2017SC1_D81.1.1.2%20CAMS-REG-v2.

Kupiainen, K., Ritola, R., Stojiljkovic, A., Pirjola, L., Malinen, A., Niemi, J., 2016. Contribution of mineral dust sources to street side ambient and suspension PM10 samples. Atmos. Environ. 147, 178–189. https://doi.org/10.1016/j.atmosenv.2016.09.059.

Lai, C., Liu, Y., Ma, J., Ma, Q., He, H., 2014. Degradation kinetics of levoglucosan initiated by hydroxyl radical under different environmental conditions. Atmos. Environ. 91, 32–39. https://doi.org/10.1016/j.atmosenv.2014.03.054.

Lawrence, S., Sokhi, R., Ravindra, K., 2016. Quantification of vehicle fleet PM10 particulate matter emission factors from exhaust and non-exhaust sources using tunnel measurement techniques. Environ. Pollut. 210, 419–428. https://doi.org/10.1016/j.envpol.2016.01.011.

Ledoux, F., Roche, C., Delmaire, G., Roussel, G., Favez, O., Fadel, M., Courcot, D., 2023. Measurement report: a 1-year study to estimate maritime contributions to PM10 in a coastal area in northern France. Atmos. Chem. Phys. 23 (15), 8607–8622. https://doi.org/10.5194/acp-23-8607-2023.

Leni, Z., Cassagnes, L.E., Daellenbach, K.R., Haddad, I. El, Vlachou, A., Uzu, G., Prévôt, A.S.H., Jaffrezo, J.L., Baumlin, N., Salathe, M., Baltensperger, U., Dommen, J., Geiser, M., 2020. Oxidative stress-induced inflammation in susceptible airways by anthropogenic aerosol. PLoS One 15 (11 November). https://doi.org/10.1371/journal.pone.0233425.

Liang, R., Chen, R., Yin, P., van Donkelaar, A., Martin, R.V., Burnett, R., Cohen, A.J., Brauer, M., Liu, C., Wang, W., Lei, J., Wang, L., Wang, L., Zhang, M., Kan, H., Zhou, M., 2022. Associations of long-term exposure to fine particulate matter and its constituents with cardiovascular mortality: a prospective cohort study in China. Environ. Int. 162, 107156. https://doi.org/10.1016/J.ENVINT.2022.107156.

Liu, Q., Baumgartner, J., Zhang, Y., Liu, Y., Sun, Y., Zhang, M., 2014. Oxidative potential and inflammatory impacts of source apportioned ambient air pollution in Beijing. Environ. Sci. Technol. 48 (21), 12920–12929. https://doi.org/10.1021/ES5029876.

Liu, T., Chan, A.W.H., Abbatt, J.P.D., 2021. Multiphase oxidation of Sulfur dioxide in aerosol particles: implications for sulfate formation in polluted environments. Environ. Sci. Technol. 55 (8), 4227–4242. https://doi.org/10.1021/ACS.EST.0C06496.

Manders, A.M.M., Builtjes, P.J.H., Curier, L., Gon, H.A.C.D.V., Hendriks, C., Jonkers, S., Kranenburg, R., Kuenen, J.J.P., Segers, A.J., Timmermans, R.M.A., Visschedijk, A.J. H., Kruit, R.J.W., Pul, W.A.J.V., Sauter, F.J., Van Der Swaluw, E., Swart, D.P.J., Douros, J., Eskes, H., Van Meijgaard, E., et al., 2017. Curriculum vitae of the LOTOS-EUROS (v2.0) chemistry transport model. Geosci. Model Dev. (GMD) 10 (11). https://doi.org/10.5194/gmd-10-4145-2017.

Manders, A., Timmermans, R., Nordmann, S., Cuesta, A., Pfaefflin, F., Schaap, M., 2021. Improving Black Carbon Modeling: Emissions and Model Evaluation - 10th International Workshop on Air Quality Forecasting Research (20-October 22, 2021).

Meteo-France. (2013). *Meteo-France weather reports*. Available at: http://bibliotheque.meteo.fr/exl-php/cadcgp.php?CMD=CHERCHE&MODELE=vues/mf_-_internet_recherche_avancee_anonyme/tpl-r.html&WHERE_IS_DOC_REF_LIT=DOC00026743&&TABLE=ILS_DOC.

Moreno-Ríos, A.L., Tejeda-Benítez, L.P., Bustillo-Lecompte, C.F., 2022. Sources, characteristics, toxicity, and control of ultrafine particles: an overview. Geosci. Front. 13 (1), 101147. https://doi.org/10.1016/J.GSF.2021.101147.

Mues, A., Kuenen, J., Hendriks, C., Manders, A., Segers, A., Scholz, Y., Hueglin, C., Builtjes, P., Schaap, M., 2014. Sensitivity of air pollution simulations with LOTOS-EUROS to the temporal distribution of anthropogenic emissions. Atmos. Chem. Phys. 14 (2), 939–955. https://doi.org/10.5194/acp-14-939-2014.

Ngoc Thuy, V.D., Jaffrezo, J.-L., Hough, I., Dominutti, P.A., Salque Moreton, G., Gille, G., Francony, F., Patron-Anquez, A., Favez, O., Uzu, G., 2024. Unveiling the optimal regression model for source apportionment of the oxidative potential of PM 10. Atmos. Chem. Phys. 24 (12), 7261–7282. https://doi.org/10.5194/acp-24-7261-2024.

Pant, P., Shi, Z., Pope, F.D., Harrison, R.M., 2017. Characterization of Traffic-Related Particulate Matter Emissions in a Road Tunnel in Birmingham, UK: Trace Metals and Organic Molecular Markers. Aerosol Air Qual. Res. 17, 117–130. https://doi.org/10.4209/aaqr.2016.01.0040.

Park, M., Soo Joo, H., Lee, K., Jang, M., Don Kim, S., Kim, I., Joanna Borlaza, L.S., Lim, H., Shin, H., Hyuck Chung, K., Choi, Y.-H., Gu Park, S., Bae, M.-S., Lee, J., Song, H., Park, K., 2018. Differential toxicities of fine particulate matters from various sources OPEN. https://doi.org/10.1038/s41598-018-35398-0.

Pietrogrande, M.C., Romanato, L., Russo, M., 2022. Synergistic and antagonistic effects of aerosol components on its oxidative potential as predictor of particle toxicity. Toxics 10 (4). https://doi.org/10.3390/TOXICS10040196.

Pio, C., Cerqueira, M., Harrison, R.M., Nunes, T., Mirante, F., Alves, C., Oliveira, C., Sanchez de la Campa, A., Artíñano, B., Matos, M., 2011. OC/EC ratio observations in Europe: Re-thinking the approach for apportionment between primary and secondary organic carbon. Atmos. Environ. 45 (34), 6121–6132. https://doi.org/10.1016/J.ATMOSENV.2011.08.045.

Pommier, M., Fagerli, H., Schulz, M., Valdebenito, A., Kranenburg, R., Schaap, M., 2020. Prediction of source contributions to urban background PM10 concentrations in European cities: a case study for an episode in December 2016 using EMEP/MSC-W rv4.15 and LOTOS-EUROS v2.0 - Part 1: the country contributions. Geosci. Model Dev. (GMD) 13 (4), 1787–1807. https://doi.org/10.5194/GMD-13-1787-2020.

Pültz, J., Banzhaf, S., Thürkow, M., Kranenburg, R., Schaap, M., 2023. Source attribution of particulate matter in Berlin. Atmos. Environ. 292, 119416. https://doi.org/10.1016/J.ATMOSENV.2022.119416.

Salameh, D., Detournay, A., Pey, J., Pérez, N., Liguori, F., Saraga, D., Bove, M.C., Brotto, P., Cassola, F., Massabò, D., Latella, A., Pillon, S., Formenton, G., Patti, S., Armengaud, A., Piga, D., Jaffrezo, J.L., Bartzis, J., Tolis, E., et al., 2015. PM2.5 chemical composition in five European Mediterranean cities: a 1-year study. Atmos. Res. 155, 102–117. https://doi.org/10.1016/j.atmosres.2014.12.001.

Samaké, A., Jaffrezo, J.L., Favez, O., Weber, S., Jacob, V., Canete, T., Albinet, A., Charron, A., Riffault, V., Perdrix, E., Waked, A., Golly, B., Salameh, D., Chevrier, F., Miguel Oliveira, D., Besombes, J.L., Martins, J.M.F., Bonnaire, N., Conil, S., et al., 2019. Arabitol, mannitol, and glucose as tracers of primary biogenic organic aerosol: the influence of environmental factors on ambient air concentrations and spatial distribution over France. Atmos. Chem. Phys. 19 (16), 11013–11030. https://doi.org/10.5194/ACP-19-11013-2019.

Samake, A., Uzu, G., Martins, J.M.F., Calas, A., Vince, E., Parat, S., Jaffrezo, J.L., 2017. The unexpected role of bioaerosols in the Oxidative Potential of PM. Scientific Reports 2017 7 (1), 1–10. https://doi.org/10.1038/s41598-017-11178-0, 7(10978).

Schaap, M., Kranenburg, R., Curier, L., Jozwicka, M., Dammers, E., Timmermans, R., 2013. Assessing the sensitivity of the OMI-NO2 product to emission changes across europe. Remote Sens. 5 (9), 4187–4208. https://doi.org/10.3390/rs5094187.

Schaap, M., Spindler, G., Schulz, M., Acker, K., Maenhaut, W., Berner, A., Wieprecht, W., Streit, N., Müller, K., Brüggemann, E., Chi, X., Putaud, J.P., Hitzenberger, R., Puxbaum, H., Baltensperger, U., Ten Brink, H., 2004. Artefacts in the sampling of nitrate studied in the "iNTERCOMP" campaigns of EUROTRAC-AEROSOL. Atmos. Environ. 38 (38), 6487–6496. https://doi.org/10.1016/j.atmosenv.2004.08.026.

Schauer, J.J., Kleeman, M.J., Cass, G.R., Simoneit, B.R.T., 2001. Measurement of emissions from air pollution sources. 3. C1-C29 organic compounds from fireplace combustion of wood. Environ. Sci. Technol. 35 (9), 1716–1728. https://doi.org/10.1021/ES001331E.

Schmidl, C., Marr, I.L., Caseiro, A., Kotianová, P., Berner, A., Bauer, H., Kasper-Giebl, A., Puxbaum, H., 2008. Chemical characterisation of fine particle emissions from wood stove combustion of common woods growing in mid-European Alpine regions. Atmos. Environ. 42 (1), 126–141. https://doi.org/10.1016/J.ATMOSENV.2007.09.028.

Sesartic, A., Dallafior, T.N., 2011. Global fungal spore emissions, review and synthesis of literature data. Biogeosciences 8 (5), 1181–1192. https://doi.org/10.5194/BG-8-1181-2011.

Simpson, D., Benedictow, A., Berge, H., Bergström, R., Emberson, L.D., Fagerli, H., Flechard, C.R., Hayman, G.D., Gauss, M., Jonson, J.E., Jenkin, M.E., Nyúri, A., Richter, C., Semeena, V.S., Tsyro, S., Tuovinen, J.P., Valdebenito, A., Wind, P., 2012. The EMEP MSC-W chemical transport model – technical description. Atmos. Chem. Phys. 12 (16), 7825–7865. https://doi.org/10.5194/ACP-12-7825-2012.

Simpson, D., Kuenen, J., Fagerli, H., Heinesen, D., Benedictow, A., Denier van der Gon, H., Visschedijk, A., Klimont, Z., Aas, W., Lin, Y., YttriK, E., Paunu, V., 2022. Revising PM2.5 emissions from residential combustion. 2005–2019: Implications for Air Quality Concentrations and Trends. Nordic Council of Ministers. https://pub.norden.org/temanord2022-540/#108663.

Stern, R., Builtjes, P., Schaap, M., Timmermans, R., Vautard, R., Hodzic, A., Memmesheimer, M., Feldmann, H., Renner, E., Wolke, R., Kerschbaumer, A., 2008. A model inter-comparison study focussing on episodes with elevated PM10 concentrations. Atmos. Environ. 42 (19), 4567–4588. https://doi.org/10.1016/j.atmosenv.2008.01.068.

Suarez-Bertoa, R., Zardini, A.A., Platt, S.M., Hellebust, S., Pieber, S.M., El Haddad, I., Temime-Roussel, B., Baltensperger, U., Marchand, N., Prévôt, A.S.H., Astorga, C., 2015. Primary emissions and secondary organic aerosol formation from the exhaust of a flex-fuel (ethanol) vehicle. Atmos. Environ. 117, 200–211. https://doi.org/10.1016/J.ATMOSENV.2015.07.006.

Thürkow, M., Banzhaf, S., Butler, T., Pültz, J., Schaap, M., 2023. Source attribution of nitrogen oxides across Germany: comparing the labelling approach and brute force technique with LOTOS-EUROS. Atmos. Environ. 292, 119412. https://doi.org/10.1016/J.ATMOSENV.2022.119412.

Tilgner, A., Schaefer, T., Alexander, B., Barth, M., Collett, J.L., Fahey, K.M., Nenes, A., Pye, H.O.T., Herrmann, H., McNeill, V.F., 2021. Acidity and the multiphase chemistry of atmospheric aqueous particles and clouds. Atmos. Chem. Phys. 21 (17), 13483–13536. https://doi.org/10.5194/ACP-21-13483-2021.

Timmermans, R., Kranenburg, R., Manders, A., Hendriks, C., Segers, A., Dammers, E., Denier van der Gon, H., Schaap, M., Dammers, E., Zhang, Q., Wang, L., Liu, Z., 2017. Source apportionment of PM2.5 across China using LOTOS-EUROS. Atmos. Environ. 164. https://doi.org/10.1016/j.atmosenv.2017.06.003.

Timmermans, R., van Pinxteren, D., Kranenburg, R., Hendriks, C., Fomba, K.W., Herrmann, H., Schaap, M., 2022. Evaluation of modelled LOTOS-EUROS with observational based PM10 source attribution. Atmos. Environ. X 14, 100173. https://doi.org/10.1016/J.AEAOA.2022.100173.

Tokaya, J.P., Kranenburg, R., Timmermans, R.M.A., Coenen, P.W.H.G., Kelly, B., Hullegie, J.S., Megaritis, T., Valastro, G., 2024. The impact of shipping on the air quality in European port cities with a detailed analysis for Rotterdam. Atmos. Environ. X 23, 100278. https://doi.org/10.1016/J.AEAOA.2024.100278.

Uzu, G., Sauvain, J.J., Baeza-Squiban, A., Riediker, M., Sánchez Sandoval Hohl, M., Val, S., Tack, K., Denys, S., Pradère, P., Dumat, C., 2011. In vitro assessment of the pulmonary toxicity and gastric availability of lead-rich particles from a lead recycling plant. Environ. Sci. Technol. 45 (18), 7888–7895. https://doi.org/10.1021/es200374c.

Valavanidis, A., Fiotakis, K., Vlachogianni, T., 2008. Airborne particulate matter and human health: toxicological assessment and importance of size and composition of particles for oxidative damage and carcinogenic mechanisms. J. Environ. Sci. Health C Environ. Carcinog. Ecotoxicol. Rev. 26 (4), 339–362. https://doi.org/10.1080/10590500802494538.

Vida, M., Foret, G., Siour, G., Couvidat, F., Favez, O., Cholakian, A., Conil, S., Beekmann, M., Jaffrezo, J.-L., 2024. Modelling of Atmospheric Concentrations of Fungal Spores: a Two-Year Simulation over France Using CHIMERE, 2. https://doi.org/10.5194/egusphere-2024-698.

Vida, M., Foret, G., Siour, G., Jaffrezo, J.L., Favez, O., Cholakian, A., Cozic, J., Dupont, H., Gille, G., Oppo, S., Zhang, S., Francony, F., Pallares, C., Conil, S., Uzu, G., Beekmann, M., 2025. Modelling oxidative potential of atmospheric particle: a 2-year study over France. Sci. Total Environ. 967 (January). https://doi.org/10.1016/j.scitotenv.2025.178813.

Wang, W., Liu, M., Wang, T., Song, Y., Zhou, L., Cao, J., Hu, J., Tang, G., Chen, Z., Li, Z., Xu, Z., Peng, C., Lian, C., Chen, Y., Pan, Y., Zhang, Y., Sun, Y., Li, W., Zhu, T., et al., 2021. Sulfate formation is dominated by manganese-catalyzed oxidation of SO2 on aerosol surfaces during haze events. Nat. Commun. 12 (1), 1–10. https://doi.org/10.1038/s41467-021-22091-6, 2021 12:1.

Weber, S., Salameh, D., Albinet, A., Alleman, L.Y., Waked, A., Besombes, J.L., Jacob, V., Guillaud, G., Meshbah, B., Rocq, B., Hulin, A., Dominik-Sègue, M., Chrétien, E., Jaffrezo, J.L., Favez, O., 2019. Comparison of PM10 sources profiles at 15 French sites using a harmonized constrained positive Matrix factorization approach. Atmosphere 10 (6), 310. https://doi.org/10.3390/ATMOS10060310, 2019, Vol. 10, Page 310.

Weber, S., Uzu, G., Favez, O., Borlaza, L.J.S., Calas, A., Salameh, D., Chevrier, F., Allard, J., Besombes, J.L., Albinet, A., Pontet, S., Mesbah, B., Gille, G., Zhang, S., Pallares, C., Leoz-Garziandia, E., Jaffrezo, J.L., 2021. Source apportionment of atmospheric PM10 oxidative potential: synthesis of 15 year-round urban datasets in France. Atmos. Chem. Phys. 21 (14), 11353–11378. https://doi.org/10.5194/ACP-21-11353-2021.

Weichenthal, S., Lavigne, E., Evans, G., Pollitt, K., Burnett, R.T., 2016. Ambient PM2.5 and risk of emergency room visits for myocardial infarction: impact of regional PM2.5 oxidative potential: a case-crossover study. Environ. Health: A Global Access Science Source 15 (1), 1–9. https://doi.org/10.1186/S12940-016-0129-9/TABLES/1.

Weilenmann, M., Favez, J.Y., Alvarez, R., 2009. Cold-start emissions of modern passenger cars at different low ambient temperatures and their evolution over vehicle legislation categories. Atmos. Environ. 43 (15), 2419–2429. https://doi.org/10.1016/J.ATMOSENV.2009.02.005.

WHO, 2022. Ambient (Outdoor) Air Pollution. Available at: https://www.who.int/news-room/fact-sheets/detail/ambient-(outdoor)-air-quality-and-health.

Ye, C., Lu, K., Song, H., Mu, Y., Chen, J., Zhang, Y., 2023. A critical review of sulfate aerosol formation mechanisms during winter polluted periods. J. Environ. Sci. (China) 123, 387–399. https://doi.org/10.1016/j.jes.2022.07.011.